 CMES, vol.56, no.1, pp.43-84, 2010

Dynamic Stress Intensity Factors of Mode I Crack Problem for Functionally Graded Layered Structures

Sheng-Hu Ding[1,2], Xing Li[2] and Yue-Ting Zhou[2,3]

Abstract: In this paper, the crack-tip fields in bonded functionally graded finite strips are studied. Different layers may have different nonhomogeneity properties in the structure. A bi-parameter exponential function was introduced to simulate the continuous variation of material properties. The problem was reduced as a system of Cauchy singular integral equations of the first kind by Laplace and Fourier integral transforms. Various internal cracks and edge crack and crack crossing the interface configurations are investigated, respectively. The asymptotic stress field near the tip of a crack crossing the interface is examined and it is shown that, unlike the corresponding stress field in piecewise homogeneous materials, in this case the "kink" in material property at the interface does not introduce any singularity. The influences of geometrical and physical parameters and crack interactions on the dynamic stress intensity factors were illustrated and discussed.

Keywords: Functionally graded layered structures; Collinear cracks; Singular integral equation; Dynamic stress intensity factor

1 Introduction

Functionally graded materials (FGMs) for high temperature applications are special composites usually made from ceramics and metals so as to achieve high toughness at high temperatures. Due to their continuously varying features of physical and mechanical properties, FGMs are quite effective to reduce the thermal and residual stresses and enhance the bonding strength.

The knowledge of the crack growth in FGMs is important in order to evaluate their integrity. Considerable investigations [Ching et al. (2001); Atluri and Shen (2002); Hsueh and Leeb (2003); Sladek et al. (2003, 2005); Han et al (2006); Zhou et al

[1] Corresponding author. Tel.: +86 951 2061405; fax: +86 951 2061405. Email: dsh-sjtu2009@163.com

[2] Department of Mathematics and Computer Science, Ningxia University, Yinchuan, 750021, China

[3] LSEC, ICMSEC, Academy of Mathematics and Systems Science, CAS, Beijing 100190, China

(2007); Wen et al. (2008); Oyekoya et al. (2008); Zhou et al. (2009)] have been made in understanding the behavior of FGMs subjected to thermal or mechanical loading conditions. To establish the fundamental relationship between material gradation and thermomechanical properties of FGMs, extensive studies have been carried out of the effective properties [Aboudi et al. (1994); Zuiker and Dvorak (1994)] the investigations of thermal properties [Ching et al. (2006); Sladek et al. (2008)] and fracture in functionally graded materials [Delale and Erdogan (1988); Erdogan and Wu (1996); Chen and Erdogan (1996); Jin and Batra (1996); Erdogan and Wu (1997); Dag and Erdogan (2002); Guo et al. (2004a,b); Kubair and Bhanu-Chandar (2007); Guo and Noda (2008); Choi and Paulino (2008)]. [Delale and Erdogan (1983)] investigated the crack problem of an infinite nonhomogeneous plate with the elastic properties varying in the direction parallel to the crack. They found that the effect of the Poisson's ratio on the stress intensity factors can be ignored. [Erdogan and Wu (1996, 1997)] studied a single functionally graded strip with an internal or edge crack. [Guo et al. (2004a)] analyzed the surface crack problem of a functionally graded orthotropic plate.

It should be mentioned that most FGMs will be used in critical situations, such as dynamic loading. But the dynamic fracture behavior of FGMs has received little attention from the scientific community. [Atkinson (1975)] first studied the crack propagation in media with spatially varying elastic properties. [Li et al. (2001)] studied the dynamic response of a finite crack in an unbounded FGM subjected to an antiplane shear loading. The variation of the shear modulus of the functionally graded material was modeled by a quadratic increase along the direction perpendicular to the crack surface. [Li and Weng (2001)] investigated the dynamic stress intensity factor of a cylindrical interface crack located between two coaxial dissimilar homogeneous cylinders that are bonded with a functionally graded interlayer and subjected to a torsional impact loading. The transient response of a functionally graded coating-substrate system with an internal or edge crack perpendicular to the interface has been studied under an in-plane impact [Guo et al. (2004b)]. Recently, [Wang and Mai (2006)] considered a periodic array of cracks in an infinite functionally graded material under transient mechanical loading. [Ding and Li (2008a)] studied a periodic array of cracks between a functionally graded material and an elastic substrate under antiplane shear loads. The dynamic fracture problem of the weak-discontinuous interface between a FGM coating and a FGM substrate have been studied by [Li et al. (2006, 2008a)].

In the foregoing studies, the functionally graded layered structures with a crack (or cracks) paralleling or perpendicular to the interface or free surface have been studied. However, there are also some other kinds of researches. By means of the Schmidt method, [Ma et al. (2005)] investigated the dynamic behavior of a finite

crack in the functionally graded materials subjected to the normally incident elastic time harmonic waves. The impact response of an inclined edge crack in a layered medium with a functionally graded interfacial zone is investigated under the state of antiplane deformation [Choi (2007a,b)]. The mixed-mode fracture problem of nonhomogeneous materials are studied by using finite element method and meshless method [So et al. (2004); Sladek et al. (2007); Liu and Yu (2008); Yu and Huang (2008); Liu et al. (2009); Minutolo et al. (2009); Sethuraman and Rajesh (2009); Shin et al. (2009)].

So many investigations have been conducted on the crack problems in functionally graded structures. However, the material properties such as shear modulus of FGMs are always assumed to be in the single-parameter exponential form. In fact, the single-parameter exponential function can only simulate special variations of material properties. A new bi-parameter exponential function was introduced to simulate the continuous variation of material properties for a weak-discontinuous interface in a symmetrical functionally gradient composite strip [Li et al. (2008b)]. The focus of the present paper is, therefore, to provide a bi-parameter exponential functions model for two collinear cracks in bonded dissimilar FGM materials under an in-plane impact. In a bi-FGM structure, both the two FGMs might have cracks along the direction of material gradient, and these cracks are parallel to one another. For these cracks, the most dangerous is a special case that there are two collinear cracks on the two sides of and perpendicular to the bi-FGM interface. The problem was reduced as a system of Cauchy singular integral equations of the first kind by Laplace and Fourier integral transforms [Ding and Li (2008b,c); Zhou et al (2008); Li (2008)]. The variations of the dynamic stress intensity factors (DSIFs) with the nonhomogeneity constants have also been depicted when the crack crossing the interface of functionally graded structures. The influences of geometrical and physical parameters on the dynamic stress intensity factor were analyzed. The present model can be reduced to a functionally graded coating-substrate structure with a crack in the coating or the homogeneous substrate or intersecting the interface, which can be used to study many kinds of problems and may be significant for the fracture mechanics analysis and design of functionally graded structures.

2 Formulation of the problem

Illustrated is a functionally graded layered structure with two collinear cracks, as shown in Fig.1. The superscript k indicates the FGM strips 1 and 2, which referred to as FGM_I and FGM_{II} respectively. Both of two layers may be nonhomogeneous and the mechanical properties are continuous across the interface. The layers are infinite in the y direction. By adjusting the thickness, h_1 and h_2, of layered structure, the model in Fig.1 can be generalized to represent a FGM coating with finite

thickness bonded to a FGM substrate with finite or infinite thickness, or two bonded functionally gradient half planes.

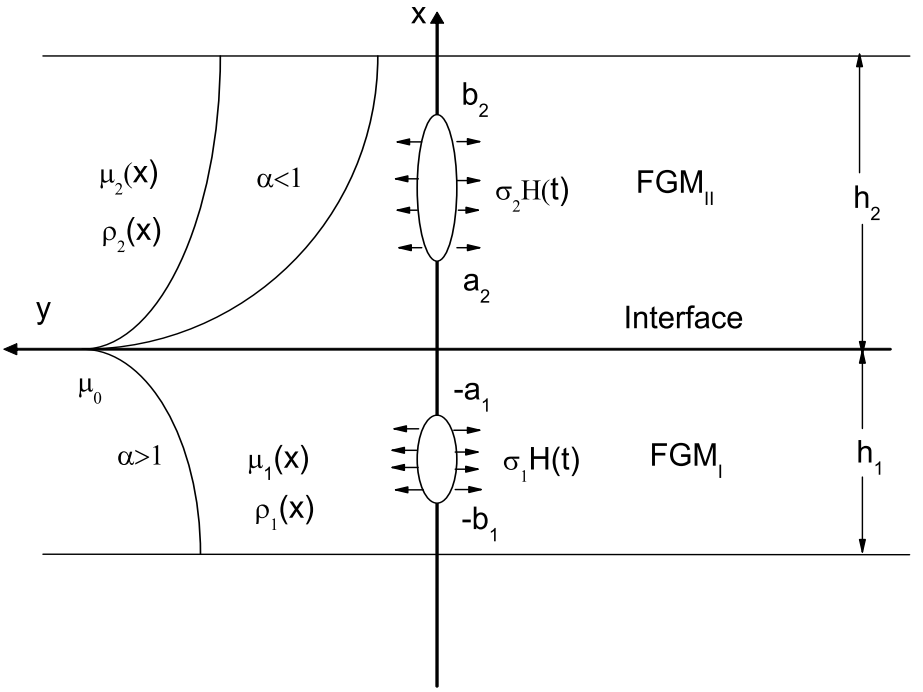

Figure 1: Geometry of collinear cracks of a FGM coating bonded to a FGM substrate

The constitutive relation of the plane problem of the functionally gradient elastic material is as follows

$$\begin{aligned}
\sigma_{xx} &= \frac{\mu(x)}{\kappa-1}[(1+\kappa)\frac{\partial u(x,y)}{\partial x}+(3-\kappa)\frac{\partial v(x,y)}{\partial y}],\\
\sigma_{yy} &= \frac{\mu(x)}{\kappa-1}[(3-\kappa)\frac{\partial u(x,y)}{\partial x}+(1+\kappa)\frac{\partial v(x,y)}{\partial y}],\\
\tau_{xy} &= \mu(x)[\frac{\partial u(x,y)}{\partial y}+\frac{\partial v(x,y)}{\partial x}],
\end{aligned} \tag{1}$$

where $\mu(x)$ is shear moduli of the nonhomogeneous materials, τ_{xy}, σ_{xx} and σ_{yy} are stress components. $u(x,y)$ and $v(x,y)$ are the displacement components in the x-direction and y-direction, $\kappa = 3-4\nu$ for plane strain, $\kappa = (3-\nu)/(1+\nu)$ for plane stress, and ν is the Poisson's ratio.

In existing papers, properties such as shear modulus of FGMs are always assumed to be in the single-parameter exponential form [Guo et al. (2004b); Wang and Mai (2006); Guo and Noda (2008); Li et al. (2008a)], which can be shown as

$$\mu(x) = \mu_0 e^{\beta x}, \quad \rho(x) = \rho_0 e^{\beta x}, \tag{2}$$

where μ_0 and ρ_0 are the shear modulus and mass density at the interface, β is the non-homogeneity parameter and x is the coordinate.

In fact, the single-parameter exponential function in Eq.(2) can only simulate special variations of material properties. In order to simulate more general variations of them, the following bi-parameter exponential functions are introduced here to express the continuous variations of the shear modulus of both FGM layers in Fig.1,

$$\mu_1(x) = \mu_0 \alpha_1^{\beta_1 x}, \quad \rho_1(x) = \rho_0 \alpha_1^{\beta_1 x}, \quad \mu_2(x) = \mu_0 \alpha_2^{\beta_2 x}, \quad \rho_2(x) = \rho_0 \alpha_2^{\beta_2 x}, \tag{3}$$

where β_1 and β_2 are two nonhomogeneous constants, and α_1 and α_2 are additional dimensionless non-homogeneity parameters. The shear modulus μ_0 and mass density ρ_0 are assigned at the interface.

The motion equations of the functionally gradient elastic material are

$$\frac{\partial \sigma_{xx}}{\partial x} + \frac{\partial \tau_{xy}}{\partial y} = \rho_0 \alpha_k^{\beta_k x} \frac{\partial^2 u}{\partial t^2}, \quad \frac{\partial \sigma_{yy}}{\partial y} + \frac{\partial \tau_{xy}}{\partial x} = \rho_0 \alpha_k^{\beta_k x} \frac{\partial^2 v}{\partial t^2}. \tag{4}$$

Introducing Laplace transform pair as follows

$$\widehat{f}(p) = \int_0^\infty f(\tau) \exp(-p\tau) d\tau, \quad f(\tau) = \frac{1}{2\pi i} \int_{Br} \widehat{f}(p) \exp(p\tau) dp, \tag{5}$$

in which Br stands for the Bromwich path of integration.

Using (1), (4) and (5) we obtain

$$\begin{aligned}
&(1+\kappa)\frac{\partial^2 \widehat{u}^{(k)}}{\partial x^2} + (\kappa-1)\frac{\partial^2 \widehat{u}^{(k)}}{\partial y^2} + 2\frac{\partial^2 \widehat{v}^{(k)}}{\partial x \partial y} + \beta_k \ln \alpha_k (1+\kappa)\frac{\partial \widehat{u}^{(k)}}{\partial x} \\
&\qquad + \beta_k \ln \alpha_k (3-\kappa)\frac{\partial \widehat{v}^{(k)}}{\partial y} = \frac{\rho_0 p^2 \widehat{u}^k (\kappa-1)}{\mu_0}, \\
&(\kappa-1)\frac{\partial^2 v^{(k)}}{\partial x^2} + (1+\kappa)\frac{\partial^2 \widehat{v}^{(k)}}{\partial y^2} + 2\frac{\partial^2 \widehat{u}^{(k)}}{\partial x \partial y} + \beta_k \ln \alpha_k (\kappa-1)\frac{\partial \widehat{v}^{(k)}}{\partial x} \\
&\qquad + \beta_k \ln \alpha_k (\kappa-1)\frac{\partial \widehat{u}^{(k)}}{\partial y} = \frac{\rho_0 p^2 \widehat{v}^k (\kappa-1)}{\mu_0},
\end{aligned} \tag{6}$$

where

$$\begin{aligned}\widehat{u}^{(k)}(x,y,p) &= \int_0^\infty u^{(k)}(x,y,t)\exp(-pt)dt,\\ \widehat{v}^{(k)}(x,y,p) &= \int_0^\infty v^{(k)}(x,y,t)\exp(-pt)dt.\end{aligned} \tag{7}$$

Here, the index k in the parentheses stand for the strips 1 and 2.
The boundary and continuity conditions are written as

$$\sigma_{xx}^{(1)}(-h_1,y,t)=0,\quad \tau_{xy}^{(1)}(-h_1,y,t)=0,\quad 0<y<\infty, \tag{8}$$

$$\sigma_{xx}^{(1)}(0,y,t)=\sigma_{xx}^{(2)}(0,y,t),\quad \tau_{xy}^{(1)}(0,y,t)=\tau_{xy}^{(2)}(0,y,t),\quad 0<y<\infty, \tag{9}$$

$$u^{(1)}(0,y,t)=u^{(2)}(0,y,t),\quad v^{(1)}(0,y,t)=v^{(2)}(0,y,t),\quad 0<y<\infty, \tag{10}$$

$$\sigma_{xx}^{(2)}(h_2,y,t)=0,\quad \tau_{xy}^{(2)}(h_2,y,t)=0,\quad 0<y<\infty, \tag{11}$$

$$\tau_{xy}^{(1)}(x,0,t)=0,\quad -h_1<x<0, \tag{12}$$

$$\tau_{xy}^{(2)}(x,0,t)=0,\quad 0<x<h_2, \tag{13}$$

$$v^{(1)}(x,0,t)=0,\quad -h_1<x<-b_1,\quad -a_1<x<0, \tag{14}$$

$$v^{(1)}(x,0,t)=0,\quad 0<x<a_2,\quad b_2<x<h_2, \tag{15}$$

$$\sigma_{yy}^{(1)}(x,0,t)=\sigma_1 H(t),\quad -b_1<x<-a_1, \tag{16}$$

$$\sigma_{yy}^{(2)}(x,0,t)=\sigma_2 H(t),\quad a_2<x<b_2. \tag{17}$$

The $\sigma_1 H(t)$ and $\sigma_2 H(t)$ are the negative of dynamic normal stress and shear stress at the crack plane under external loading in an uncracked specimen. $H(t)$ is the Heaviside function of time t. When $t<0$, $H(t)=0$, and when $t\geq 0$, $H(t)=1$.

3 Method of solutions

For the symmetry of the structure in Fig.1, it is enough to only analyze the left half part $(y>0)$. Employing the Fourier transform on Eq.(6), the the displacement

components can be expressed as

$$\begin{aligned}\widehat{u}^{(k)}(x,y,p) =& \frac{1}{2\pi}\int_{-\infty}^{\infty}\sum_{j=1}^{2} m_{kj}(s,p)A_{kj}(s,p)e^{n_{kj}y}e^{-isx}\,\mathrm{d}s \\ &+\frac{2}{\pi}\int_{0}^{\infty}\sum_{j=1}^{4} q_{kj}(\alpha,p)B_{kj}(\alpha,p)e^{p_{kj}x}\cos\alpha y\,\mathrm{d}\alpha, \\ \widehat{v}^{(k)}(x,y,p) =& \frac{1}{2\pi}\int_{-\infty}^{\infty}\sum_{j=1}^{2} A_{kj}(s,p)e^{n_{kj}y}e^{-isx}\,\mathrm{d}s \\ &+\frac{2}{\pi}\int_{0}^{\infty}\sum_{j=1}^{4} B_{kj}(\alpha,p)e^{p_{kj}x}\sin\alpha y\,\mathrm{d}\alpha,\end{aligned} \tag{18}$$

where $m_{kj}(s,p)$, n_{kj}, $q_{kj}(s,p)$ and p_{kj} $(k=1,2, j=1-4)$ can be found in Appendix A. $A_{kj}(s,p)$, $B_{kj}(\alpha,p)$ $(k=1,2, j=1-4)$ are unknowns to be solved.

Substituting (18) into (1), the stress components are obtained as

$$\begin{aligned}\widehat{\sigma}_{xx}^{(k)}(x,y,p) = \alpha_k^{\beta_k x}\Bigg(&\frac{1}{2\pi}\int_{-\infty}^{\infty}\sum_{j=1}^{2} c_{kj}(s,p)A_{kj}(s,p)e^{n_{kj}y}e^{-isx}\,\mathrm{d}s \\ &+\frac{2}{\pi}\int_{0}^{\infty}\sum_{j=1}^{4} c_{(k+2)j}(\alpha,p)B_{kj}(\alpha,p)e^{p_{kj}x}\cos\alpha y\,\mathrm{d}\alpha\Bigg),\end{aligned} \tag{19}$$

$$\begin{aligned}\widehat{\sigma}_{yy}^{(k)}(x,y,p) = \alpha_k^{\beta_k x}\Bigg(&\frac{1}{2\pi}\int_{-\infty}^{\infty}\sum_{j=1}^{2} d_{kj}(s,p)A_{kj}(s,p)e^{n_{kj}y}e^{-isx}\,\mathrm{d}s \\ &+\frac{2}{\pi}\int_{0}^{\infty}\sum_{j=1}^{4} d_{(k+2)j}(\alpha,p)B_{kj}(\alpha,p)e^{p_{kj}x}\cos\alpha y\,\mathrm{d}\alpha\Bigg),\end{aligned} \tag{20}$$

$$\begin{aligned}\widehat{\tau}_{xy}^{(k)}(x,y,p) = \alpha_k^{\beta_k x}\Bigg(&\frac{1}{2\pi}\int_{-\infty}^{\infty}\sum_{j=1}^{2} e_{kj}(s,p)A_{kj}(s,p)e^{n_{kj}y}e^{-isx}\,\mathrm{d}s \\ &+\frac{2}{\pi}\int_{0}^{\infty}\sum_{j=1}^{4} e_{(k+2)j}(\alpha,p)B_{kj}(\alpha,p)e^{p_{kj}x}\sin\alpha y\,\mathrm{d}\alpha\Bigg),\end{aligned} \tag{21}$$

where

$$\begin{aligned}\widehat{\sigma}_{xx}^{(k)}(x,y,p) &= \int_0^{\infty}\sigma_{xx}^{(k)}(x,y,t)\exp(-pt)dt, \\ \widehat{\sigma}_{yy}^{(k)}(x,y,p) &= \int_0^{\infty}\sigma_{yy}^{(k)}(x,y,t)\exp(-pt)dt, \\ \widehat{\tau}_{xy}^{(k)}(x,y,p) &= \int_0^{\infty}\tau_{xy}^{(k)}(x,y,t)\exp(-pt)dt.\end{aligned} \tag{22}$$

Here, c_{kj}, d_{kj} and $e_{kj}(k=1,2, j=1-4)$ are known expressions shown in Appendix A.

Now, we define the following new unknown functions

$$\begin{aligned} \widehat{g}_1(x_1,p) &= \frac{\partial \widehat{v}^{(1)}(x_1,0,p)}{\partial x_1}, \quad -b_1 < x_1 < -a_1, \\ \widehat{g}_2(x_2,p) &= \frac{\partial \widehat{v}^{(2)}(x_2,0,p)}{\partial x_2}, \quad a_2 < x_2 < b_2, \end{aligned} \tag{23}$$

where $x = x_1$ for $x < 0$, and $x = x_2$ for $x > 0$.

From (12-15), and then substituting (23) into (18), we obtain

$$\begin{aligned} A_{11}(s,p) &= f_{11}(s,p) \int_{-b_1}^{-a_1} \widehat{g}_1(t_1,p) e^{ist_1}\, \mathrm{d}t_1, \\ A_{12}(s,p) &= f_{12}(s,p) \int_{-b_1}^{-a_1} \widehat{g}_1(t_1,p) e^{ist_1}\, \mathrm{d}t_1, \end{aligned} \tag{24}$$

$$\begin{aligned} A_{21}(s,p) &= f_{21}(s,p) \int_{a_2}^{b_2} \widehat{g}_2(t_2,p) e^{ist_2}\, \mathrm{d}t_2, \\ A_{22}(s,p) &= f_{22}(s,p) \int_{a_2}^{b_2} \widehat{g}_2(t_2,p) e^{ist_2}\, \mathrm{d}t_2, \end{aligned} \tag{25}$$

where

$$\begin{aligned} f_{11}(s,p) &= -\frac{m_{12}n_{12} - is}{m_{11}n_{11} - m_{12}n_{12}} \frac{i}{s}, \quad f_{12}(s,p) = -\frac{m_{11}n_{11} - is}{m_{11}n_{11} - m_{12}n_{12}} \frac{i}{s}, \\ f_{21}(s,p) &= -\frac{m_{22}n_{22} - is}{m_{21}n_{21} - m_{22}n_{22}} \frac{i}{s}, \quad f_{22}(s,p) = -\frac{m_{21}n_{21} - is}{m_{21}n_{21} - m_{22}n_{22}} \frac{i}{s}. \end{aligned} \tag{26}$$

By using the boundary and continuity conditions (8-11), B_{1j} and $B_{2j}(j=1-4)$ can be found according to $\widehat{g}_1(x_1,p)$ and $\widehat{g}_2(x_2,p)$

$$B_{1j}(\alpha,p) = \int_{-b_1}^{-a_1} \widehat{C}_j(t_1,\alpha,p)\widehat{g}_1(t_1,p)dt_1 + \int_{a_2}^{b_2} \widehat{D}_j(t_2,\alpha,p)\widehat{g}_2(t_2,p)dt_2, \tag{27}$$

$$B_{2j}(\alpha,p) = \int_{-b_1}^{-a_1} \widehat{C}_{j+4}(t_1,\alpha,p)\widehat{g}_1(t_1,p)dt_1 + \int_{a_2}^{b_2} \widehat{D}_{j+4}(t_2,\alpha,p)\widehat{g}_2(t_2,p)dt_2, \tag{28}$$

where $\widehat{C}_j$ and $\widehat{D}_j$ $(j=1-8)$ can be seen in Appendix B.

Using (16) and (17), the following equations can be obtained

$$\begin{aligned}
&\int_{-b_1}^{-a_1} K_{11}(x_1,t_1,p)\widehat{g}_1(t_1,p)\,\mathrm{d}t_1 + \int_{-b_1}^{-a_1} K_{12}(x_1,t_1,p)\widehat{g}_1(t_1,p)\,\mathrm{d}t_1 \\
&\qquad + \int_{a_2}^{b_2} K_{13}(x_1,t_2,p)\widehat{g}_2(t_2,p)\,\mathrm{d}t_2 = \alpha_1^{-\beta_1 x_1}\sigma_1/p, \\
&\int_{a_2}^{b_2} K_{21}(x_2,t_2,p)\widehat{g}_2(t_2,p)\,\mathrm{d}t_2 + \int_{-b_1}^{-a_1} K_{22}(x_2,t_1,p)\widehat{g}_1(t_1,p)\,\mathrm{d}t_1 \\
&\qquad + \int_{a_2}^{b_2} K_{23}(x_2,t_2,p)\widehat{g}_2(t_2,p)\,\mathrm{d}t_2 = \alpha_2^{-\beta_2 x_2}\sigma_2/p,
\end{aligned} \tag{29}$$

where

$$\begin{aligned}
K_{11}(x_1,t_1,p) &= \lim_{y\to 0}\frac{1}{2\pi}\int_{-\infty}^{\infty} k_{11}(y,s,p)e^{is(t_1-x_1)}\,\mathrm{d}s, \\
K_{12}(x_1,t_1,p) &= \lim_{y\to 0}\frac{2}{\pi}\int_{0}^{\infty} k_{12}(\alpha,x_1,t_1,p)\cos\alpha y\,\mathrm{d}\alpha, \\
K_{13}(x_1,t_2,p) &= \lim_{y\to 0}\frac{2}{\pi}\int_{0}^{\infty} k_{13}(\alpha,x_1,t_2,p)\cos\alpha y\,\mathrm{d}\alpha,
\end{aligned} \tag{30}$$

$$\begin{aligned}
K_{21}(x_2,t_2,p) &= \lim_{y\to 0}\frac{1}{2\pi}\int_{-\infty}^{\infty} k_{21}(y,s,p)e^{is(t_2-x_2)}\,\mathrm{d}s, \\
K_{22}(x_2,t_1,p) &= \lim_{y\to 0}\frac{2}{\pi}\int_{0}^{\infty} k_{22}(\alpha,x_2,t_1,p)\cos\alpha y\,\mathrm{d}\alpha, \\
K_{23}(x_2,t_2,p) &= \lim_{y\to 0}\frac{2}{\pi}\int_{0}^{\infty} k_{23}(\alpha,x_2,t_2,p)\cos\alpha y\,\mathrm{d}\alpha,
\end{aligned} \tag{31}$$

where $k_{11}(y,s,p)$, $k_{12}(\alpha,x_1,t_1,p)$, $k_{13}(\alpha,x_1,t_2,p)$, $k_{21}(y,s,p)$, $k_{22}(\alpha,x_2,t_1,p)$ and $k_{23}(\alpha,x_2,t_2,p)$ are given in Appendix C.

To derive the singular integral equation, one of the most important jobs is to conduct an asymptotic analysis. When $s\to\infty$, after lengthy manipulations the asymptotic form of $k_{11}(0,s,p)$ and $k_{21}(0,s,p)$ $(y=0)$ can be obtained as

$$k_{11\infty}(0,s,p) = -\frac{|s|}{s}\frac{4\mu_0 i}{1+\kappa} + \frac{1}{s}\frac{2\beta_1\ln\alpha_1\mu_0}{1+\kappa} + O(\frac{1}{s^2}), \tag{32}$$

$$k_{21\infty}(0,s,p) = -\frac{|s|}{s}\frac{4\mu_0 i}{1+\kappa} + \frac{1}{s}\frac{2\beta_2\ln\alpha_2\mu_0}{1+\kappa} + O(\frac{1}{s^2}). \tag{33}$$

For internal cracks $(-h_1<-b_1<-a_1<0<a_2<b_2<h_2)$, $k_{12}(\alpha,x_1,t_1,p)$, $k_{13}(\alpha,x_1,t_2,p)$, $k_{22}(\alpha,x_2,t_1,p)$, $k_{23}(\alpha,x_2,t_2,p)$ are bounded at the interval $-b_1\le x_1\le -a_1$ and $a_2\le x_2\le b_2$, but $k_{12}(\alpha,x_1,t_1,p)$, $k_{13}(\alpha,x_1,t_2,p)$, $k_{22}(\alpha,x_2,t_1,p)$, $k_{23}(\alpha,x_2,t_2,p)$

would include singular terms for edge crack ($b_1 = h_1$ or $b_2 = h_2$) or crack terminating at the interface ($a_1 = 0$ or $a_2 = 0$). After lengthy analysis, when $\alpha \to \infty$, we obain

$$k_{12\infty}(\alpha, x_1, t_1, p) \cong (b_{11}\alpha + b_{12})e^{\alpha(t_1+x_1)} + (b_{21}\alpha^2 + b_{22}\alpha + b_{23})e^{-\alpha(2h_1+t_1+x_1)}, \tag{34}$$

$$k_{13\infty}(\alpha, x_1, t_2, p) \cong (b_{31}\alpha + b_{32})e^{\alpha(x_1-t_2)}, \tag{35}$$

$$k_{22\infty}(\alpha, x_2, t_1, p) \cong (b_{41}\alpha + b_{42})e^{-\alpha(x_2-t_1)}, \tag{36}$$

$$k_{23\infty}(\alpha, x_1, t_1, p) \cong (b_{51}\alpha + b_{52})e^{-\alpha(t_2+x_2)} + (b_{61}\alpha^2 + b_{62}\alpha + b_{63})e^{-\alpha(2h_2-t_2-x_2)}, \tag{37}$$

where $b_{11}, ..., b_{63}$ are very complicated expressions, and can be found in [Ding (2009)].

From (32-37), Eq.(29) can be expressed as

$$\begin{aligned} &\frac{1}{\pi}\int_{-b_1}^{-a_1} \frac{\widehat{g}_1(t_1,p)}{t_1 - x_1}\,\mathrm{d}t_1 + \int_{-b_1}^{-a_1} H_{11}(x_1,t_1,p)\widehat{g}_1(t_1,p)\,\mathrm{d}t_1 \\ &+ \int_{a_2}^{b_2} H_{12}(x_1,t_2,p)\widehat{g}_2(t_2,p)\,\mathrm{d}t_2 = \frac{1+\kappa}{4\mu_0}\sigma_1(x_1)\alpha_1^{-\beta_1 x_1}/p, \end{aligned} \tag{38}$$

$$\begin{aligned} &\frac{1}{\pi}\int_{a_2}^{b_2} \frac{\widehat{g}_2(t_2,p)}{t_2 - x_2}\,\mathrm{d}t_2 + \int_{-b_1}^{-a_1} H_{21}(x_2,t_1,p)\widehat{g}_1(t_1,p)\,\mathrm{d}t_1 \\ &+ \int_{a_2}^{b_2} H_{22}(x_2,t_2,p)\widehat{g}_2(t_2,p)\,\mathrm{d}t_2 = \frac{1+\kappa}{4\mu_0}\sigma_2(x_2)\alpha_2^{-\beta_2 x_2}/p, \end{aligned} \tag{39}$$

where $H_{ij}(i = 1,2, j = 1,2)$ can be found in Appendix C.

4 Evaluation of singularities and expression for dynamic stress intensity factors

With the knowledge of the possible singular kernels obtained in the Section 3, we can now evaluate the singularities of the unknown kernel functions for different crack configurations.

4.1 Internal crack problem

Consider two collinear internal cracks in a FGM coating bonded to a FGM substrate (Fig.1). For this case, note that the singular term $\dfrac{1}{t-x}$ is associated with

two embedded cracks in two materials and leads to the standard square-root singularity for the unknown function $\widehat{g}_1(t_1,p)$ and $\widehat{g}_2(t_2,p)$. It may easily be shown that for $-b_1 > -h_1$ and $-a_1 < 0$, and $a_2 > 0$ and $b_2 < h_2$, $K_{ij}(i = 1,2, j = 1-3)$ remain bounded in the closed interval $-b_1 \le (x_1,t_1) \le -a_1$ and $a_2 \le (x_2,t_2) \le b_2$, respectively.

We define dimensionless quantities

$$\begin{aligned} t_1 &= u_1(b_1-a_1)/2-(b_1+a_1)/2, \quad x_1 = r_1(b_1-a_1)/2-(b_1+a_1)/2, \\ t_2 &= u_2(b_2-a_2)/2+(b_2+a_2)/2, \quad x_2 = r_2(b_2-a_2)/2+(b_2+a_2)/2. \end{aligned} \tag{40}$$

The solutions of the singular integral equations Eqs.(38) and (39) with the Cauchy type kernel are [Erdogan (1973)]

$$\widehat{g_1}(u_1,p) = G_1(u_1,p)/\sqrt{1-u_1^2}, \quad \widehat{g}_2(u_2,p) = G_2(u_2,p)/\sqrt{1-u_2^2}, \tag{41}$$

where $G_1(u_1,p)$ and $G_2(u_2,p)$ are bounded functions, which can be expressed as

$$G_1(u_1,p) = \sum_{n=0}^{\infty} A_n T_n(u_1), \quad G_2(u_2,p) = \sum_{n=0}^{\infty} B_n T_n(u_2). \tag{42}$$

Here, T_n is the Chebyshev polynomial of the first kind and A_n and B_n are unknown constants. $G_1(u_1,p)$ and $G_2(u_2,p)$ must fulfill the following single-valuedness as

$$\int_{-1}^{1} G_1(u_1,p)/\sqrt{1-u_1^2}\,\mathrm{d}u_1 = 0, \quad \int_{-1}^{1} G_2(u_2,p)/\sqrt{1-u_2^2}\,\mathrm{d}u_2 = 0. \tag{43}$$

The stress intensity factors in Laplace domain can be defined as

$$\begin{aligned} \widehat{K}_I(-b_1,p) &= \frac{4\mu_0\alpha_1^{-\beta_1 b_1}}{1+\kappa}\sqrt{(b_1-a_1)/2}G_1(-1,p), \\ \widehat{K}_I(-a_1,p) &= -\frac{4\mu_0\alpha_1^{-\beta_1 a_1}}{1+\kappa}\sqrt{(b_1-a_1)/2}G_1(1,p), \end{aligned} \tag{44}$$

$$\begin{aligned} \widehat{K}_I(a_2,p) &= \frac{4\mu_0\alpha_2^{\beta_2 a_2}}{1+\kappa}\sqrt{(b_2-a_2)/2}G_2(-1,p), \\ \widehat{K}_I(b_2,p) &= -\frac{4\mu_0\alpha_2^{\beta_2 b_2}}{1+\kappa}\sqrt{(b_2-a_2)/2}G_2(1,p). \end{aligned} \tag{45}$$

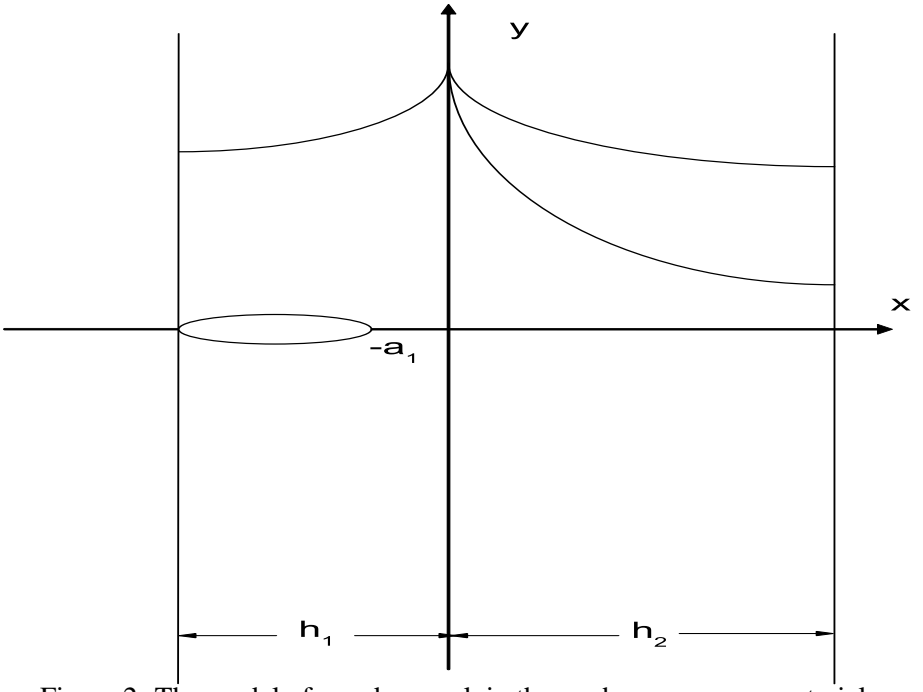

Figure 2: The model of an edge crack in the nonhomogeneous material.

4.2 Surface crack problem

Consider an edge crack in the nonhomogeneous material shown in Fig.2. For the edge crack problem ($b_1 = h_1$ or $b_2 = h_2$), we define dimensionless quantities

$$\begin{aligned} t_1 &= u_1(h_1-a_1)/2-(h_1+a_1)/2, \quad x_1 = r_1(h_1-a_1)/2-(h_1+a_1)/2, \\ t_2 &= u_2(h_2-a_2)/2+(h_2+a_2)/2, \quad x_2 = r_2(h_2-a_2)/2+(h_2+a_2)/2. \end{aligned} \tag{46}$$

The solution of Eqs.(38) and (39) may be written as [Erdogan (1973)]

$$\widehat{g}(u_1,p) = G_1(u_1,p)/\sqrt{1-u_1}, \quad \widehat{g}(u_2,p) = G_2(u_2,p)/\sqrt{1-u_2}. \tag{47}$$

where $G_1(u_1,p)$ and $G_2(u_2,p)$ are bounded functions, which can be expressed as

$$G_1(u_1,p) = \sum_{n=0}^{\infty} C_n T_n(u_1), \quad G_2(u_2,p) = \sum_{n=0}^{\infty} D_n T_n(u_2). \tag{48}$$

It should be noted that there is no single valuedness condition for the case of the edge crack. We need to choose collocation points to obtain an system of algebraic

equations. After C_n and D_n are obtained, the stress intensity factor of the edge crack tip in Laplace domain can be expressed as

$$\widehat{K}_I(-a_1,p)=-\frac{4\mu_0\alpha_1^{-\beta_1 a_1}}{1+\kappa}\sqrt{h_1-a_1}G_1(1,p),\quad \widehat{K}_I(a_2,p)=\frac{4\mu_0\alpha_2^{\beta_2 a_2}}{1+\kappa}\sqrt{h_2-a_2}G_2(1,p). \tag{49}$$

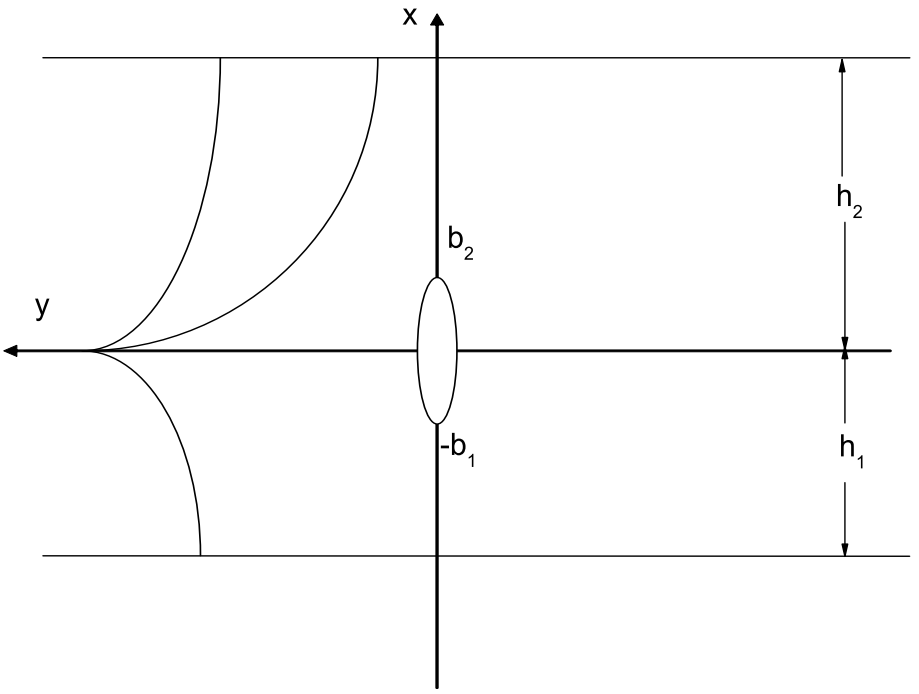

Figure 3: The geometry of crack passing through interface.

4.3 Crack passing interface problem

Since the fracture problems of FGMs with a crack crossing the interface have been scarcely studied in the past, the present work will be significant for the fracture mechanics analysis and design of functionally graded layered structures. Consider an internal crack crossing the interface shown in Fig.3. For the case of crack passing

interface problem (i.e., $a_1 = 0$ and $a_2 = 0$), Eq. (38) and (39) becomes

$$\begin{aligned} &\frac{1}{\pi}\int_{-b_1}^{0}\frac{\widehat{g}_1(t_1,p)}{t_1-x_1}\,\mathrm{d}t_1+\int_{-b_1}^{0}H_{11}(x_1,t_1,p)\widehat{g}_1(t_1,p)\,\mathrm{d}t_1\\ &+\int_{0}^{b_2}H_{12}(x_1,t_2,p)\widehat{g}_2(t_2,p)\,\mathrm{d}t_2=\frac{1+\kappa}{4\mu_0}\sigma_1(x_1)\alpha_1^{-\beta_1 x_1}/p, \end{aligned} \tag{50}$$

$$\begin{aligned} &\frac{1}{\pi}\int_{0}^{b_2}\frac{\widehat{g}_2(t_2,p)}{t_2-x_2}\,\mathrm{d}t_2+\int_{-b_1}^{0}H_{21}(x_2,t_1,p)\widehat{g}_1(t_1,p)\,\mathrm{d}t_1\\ &+\int_{0}^{b_2}H_{22}(x_2,t_2,p)\widehat{g}_2(t_2,p)\,\mathrm{d}t_2=\frac{1+\kappa}{4\mu_0}\sigma_2(x_2)\alpha_2^{-\beta_2 x_2}/p. \end{aligned} \tag{51}$$

From (32-37), Fredholm kernels $H_{11}(x_1,t_1,p)$, $H_{22}(x_2,t_2,p)$ do not contain any singular terms. However, $H_{12}(x_1,t_2,p)$, $H_{21}(x_2,t_1,p)$ do include singular terms as the coupling terms. After some analysis, the singular terms are expressed as

$$\begin{aligned} H_{12s}(x_1,t_2,p)&=\frac{1}{t_2-x_1}, \quad -h_1<x_1<0, \quad 0<t_2<h_2,\\ H_{21s}(x_2,t_1,p)&=\frac{1}{t_1-x_2}, \quad -h_1<t_1<0, \quad 0<x_2<h_2, \end{aligned} \tag{52}$$

where x_1, t_1 are always negative while x_2, t_2 are always positive. Hence $H_{12s}(x_1,t_2,p)$ is singular only when both x_1 and t_2 go to zero. Similarly, $H_{21s}(x_2,t_1,p)$ is singular only when both x_2 and t_1 go to zero.

Putting all the bounded parts to the right hand side, Eqs.(50) and (51) becomes

$$\begin{aligned} &\frac{1}{\pi}\int_{-b_1}^{0}\frac{\widehat{g}_1(t_1,p)}{t_1-x_1}\,\mathrm{d}t_1+\int_{0}^{b_2}\frac{\widehat{g}_2(t_2,p)}{t_2-x_1}\,\mathrm{d}t_2=\Phi_1(x_1,p),\\ &\frac{1}{\pi}\int_{0}^{b_2}\frac{\widehat{g}_2(t_2,p)}{t_2-x_2}\,\mathrm{d}t_2+\int_{-b_1}^{0}\frac{\widehat{g}_1(t_1,p)}{t_1-x_2}\,\mathrm{d}t_1=\Phi_2(x_2,p). \end{aligned} \tag{53}$$

Here, $\Phi_1(x_1,p)$ and $\Phi_2(x_2,p)$ represent the bounded terms. To examine the singularity, we let

$$\widehat{g}_1(t_1,p)=\frac{\overline{g_1}(t_1,p)}{(t_1+b_1)^{\omega_1}(-t_1)^{\varsigma_1}}, \quad \widehat{g}_2(t_2,p)=\frac{\overline{g_2}(t_2,p)}{(t_2)^{\omega_2}(b_2-t_2)^{\varsigma_2}}, \tag{54}$$

where $\overline{g_1}(t_1,p)$ and $\overline{g_2}(t_2,p)$ are Hölder continuous on $-b_1<t_1<0$ and $0<t_2<b_2$, respectively. It should be noted that at zero there can be only one irregular point. Therefore, $\varsigma_1=\omega_2$.

After lengthy manipulations it can be shown that [Muskhelishvili (1953)]

$$\cos(\pi\omega_1)=0, \quad \cos(\pi\varsigma_2)=0, \quad \varsigma_1=0, \quad \omega_2=0, \tag{55}$$

giving $\omega_1 = \varsigma_2 = \frac{1}{2}$. The result $\varsigma_1 = 0$ implies that there is no power singularity at the interface. There is a possibility of a logarithmic singularity. It has been verified that, the logarithmic singularity is square integrable and will not affect the singular nature of the integral equations [Erdogan et al. (1991)]. We can concluded that there is no irregular point at the interface, which is different from the case of nonsquare-root singularity for the crack touching interface between two homogeneous materials [Cook and Erdogan (1972)].

Since there is no singularity at the interface, we can pose Eqs.(50) and (51) as one singular integral equation as

$$\frac{1}{\pi}\int_{-b_1}^{b_2}\frac{\widehat{g}(t,p)}{t-x}\,\mathrm{d}t + \int_{-b_1}^{b_2} H(x,t,p)\widehat{g}(t,p)\,\mathrm{d}t = \frac{1+\kappa}{4\mu_0}\sigma(x,p), \tag{56}$$

where

$$\widehat{g}(t,p) = \begin{cases} \widehat{g}_1(t,p), & t<0, \\ \widehat{g}_2(t,p), & t>0, \end{cases} \tag{57}$$

$$H(x,t,p) = \begin{cases} H_{11}(x,t,p), & (x,t)<0, \\ H_{12}(x,t,p) - \frac{1}{t-x}, & x<0, \quad t>0, \\ H_{21}(x,t,p) - \frac{1}{t-x}, & x>0, \quad t<0, \\ H_{22}(x,t,p), & (x,t)>0, \end{cases} \tag{58}$$

$$\sigma(x,p) = \begin{cases} \sigma_1(x)\alpha_1^{-\beta_1 x}/p, & x<0, \\ \sigma_2(x)\alpha_2^{-\beta_2 x}/p, & x>0. \end{cases} \tag{59}$$

It should be noted that the only irregular points are $x=-b_1$ and $x=b_2$. Therefore, we can write

$$\widehat{g}(t,p) = G(t,p)/\sqrt{(t+b_1)(b_2-t)}, \tag{60}$$

where $G(t,p)$ is bounded function.

We defining the normalized quantities

$$t = u(b_1+b_2)/2 + (b_2-b_1)/2, \quad x = r(b_1+b_2)/2 + (b_2-b_1)/2. \tag{61}$$

The solution of Eq.(56) can be expressed as [Erdogan (1973)]

$$\widehat{g}(u,p) = G(u,p)/\sqrt{1-u^2}, \tag{62}$$

where $G(u,p)$ is bounded function, which can be expressed as

$$G(u,p) = \sum_{n=0}^{\infty} E_n T_n(u). \tag{63}$$

We can write the stress intensity factors as

$$\begin{aligned} \widehat{K}_I(-b_1,p) &= \frac{4\mu_0\alpha_1^{-\beta_1 b_1}}{1+\kappa}\sqrt{(b_1+b_2)/2}G(-1,p), \\ \widehat{K}_I(b_2,p) &= -\frac{4\mu_0\alpha_2^{\beta_2 b_2}}{1+\kappa}\sqrt{(b_1+b_2)/2}G(1,p). \end{aligned} \tag{64}$$

5 Results and discussion

The following analysis of DSIFs will be conducted, respectively, for two internal cracks and an edge crack and a internal crack crossing the interface. The surface of the two cracks loaded by $\sigma_{10}H(t)$ and $\sigma_{20}H(t)$ respectively, where σ_{10} and σ_{20} are constant tractions. Plane strain state is considered here. The DSIFs are normalized by $k_{10}=\sigma_{10}\sqrt{a_{01}}$ and $k_{20}=\sigma_{20}\sqrt{a_{02}}$ for two internal cracks and by $k_{10}=\sigma_{10}\sqrt{h_1-a_1}$ and $k_{20}=\sigma_{10}\sqrt{h_2-a_2}$ for the edge crack, where $a_{01}=(b_1-a_1)/2$ and $a_{02}=(b_2-a_2)/2$. When a internal crack passing through the interface, the DSIFs are normalized by $k_{30}=\sigma_{10}\sqrt{a_{01}}$, where $a_{01}=(b_1+b_2)/2$. The x-coordinate of the crack center is defined as $d_1=(a_1+b_1)/2$ and $d_2=(a_2+b_2)/2$ for two internal cracks, and $d_1=(a_1+h_1)/2$ and $d_2=(a_2+h_2)/2$ for the edge crack. Poisson's ratio is taken as $\nu=0.3$.

5.1 Single parameter exponential model

To verify the validity of the analytical solution procedure, we firstly restrict our attention to a functionally graded strip with a central crack vertical to the interface bonded to a homogeneous strip under static load (i.e. $a_{02}=0$, $p\to 0$ or $t\to\infty$). The corresponding static problem was studied by [Guo et al. (2004b)]. The nonhomogeneous parameter α_1 and α_2 are assumed to be equal to e. From Fig.4, it's observed that the present results coincide well with those of [Guo et al. (2004b)].

Subsequently, let us consider single crack or two collinear cracks problem. First, there was no crack in the FGM_{II}. Then a crack ranging from $0.4h_1$ to $0.6h_1$ is placed in the FGM_{II}. And then a longer crack ranging from $0.3h_1$ to $0.7h_1$ is placed. Fig.5 shows the influence of a_{02}/h_2 on the normalized DSIFs when β_2/β_1=-1.0. It can be seen that the peak value and the corresponding static value of the normalized DSIFs are minimum for single crack.

Figs.6 and 7 show the influence of nonhomogeneous parameter ratio β_1/β_2 on the normalized DSIFs when the two collinear cracks both exist in the layered structure. It can be observed that both the peak and static values of $K_I(-b_1,t)/k_{10}$ decrease with an increase of β_1/β_2. The peak and static values of $K_I(-a_1,t)/k_{10}$ increase with an increase of β_1/β_2. When $\beta_1/\beta_2>0$, the peak and corresponding static

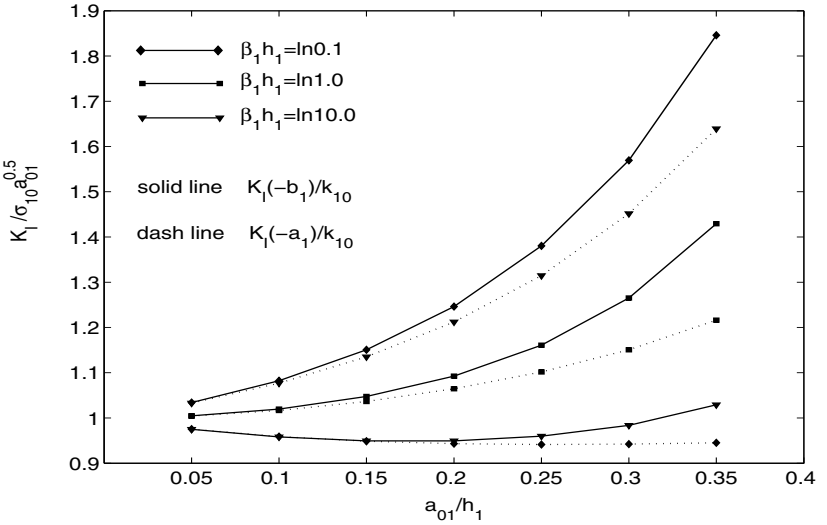

Figure 4: Influences on normalized static SIF for a central internal crack in FGM coating bonded to a homogeneous substrate ($h_2/h_1 = 1, d_1/h_1 = 0.5, a_{02} = 0.0, \beta_2 = 0.0$)

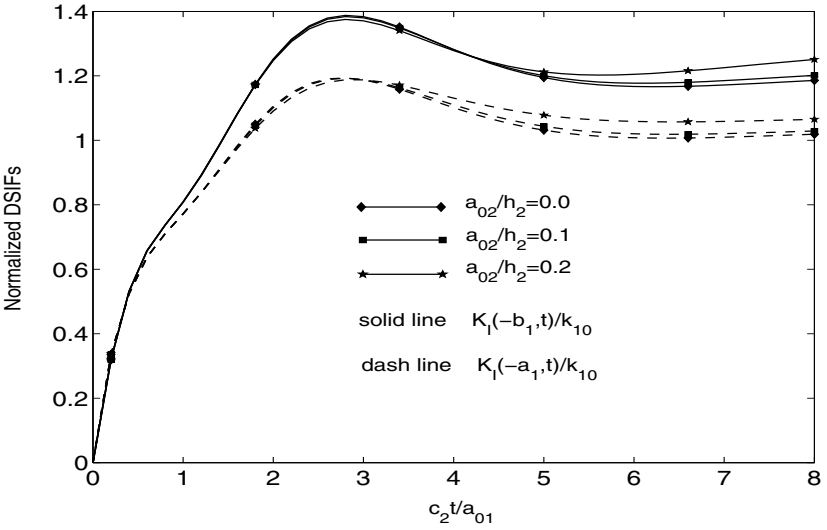

Figure 5: Influences on DSIFs for a single crack two collinear cracks in different FGMs ($h_2/h_1 = 1, d_1/h_1 = 0.5, d_2/h_2 = 0.5, \beta_1 = -\ln 2.0, \beta_2 = \ln 2.0$)

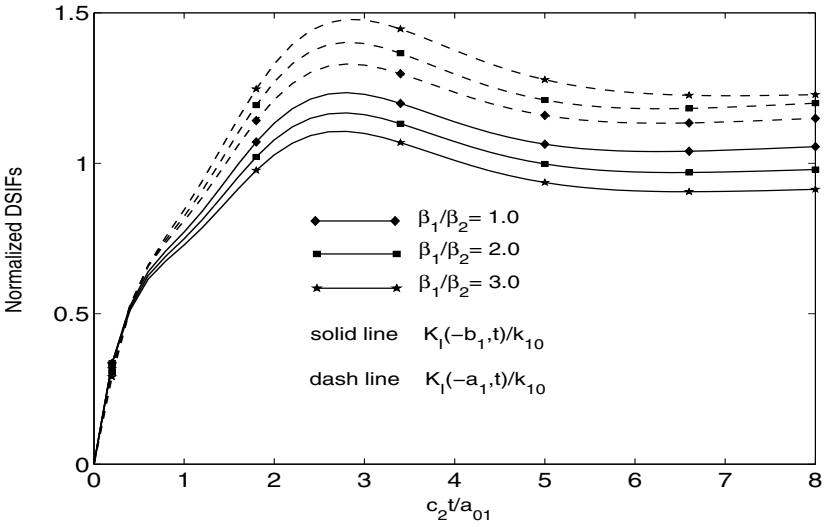

Figure 6: Influences of the ratio between the two nonhomogeneity parameters on the stress intensity factor of collinear cracks ($h_2/h_1 = 1, d_1/h_1 = 0.5, d_2/h_2 = 0.5, \beta_2 = \ln 2.0, a_{02}/h_2 = 0.2$)

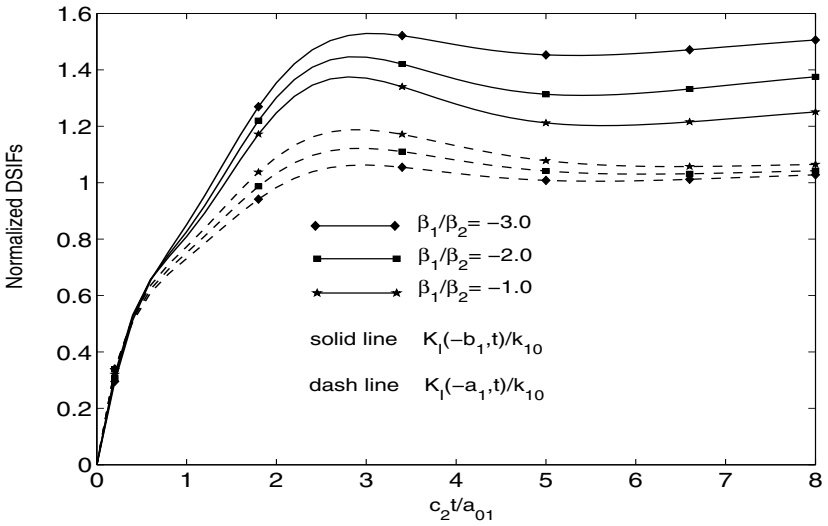

Figure 7: Influences of the ratio between the two nonhomogeneity parameters on the stress intensity factor of collinear cracks ($h_2/h_1 = 1, d_1/h_1 = 0.5, d_2/h_2 = 0.5, \beta_2 = \ln 2.0, a_{02}/h_2 = 0.2$)

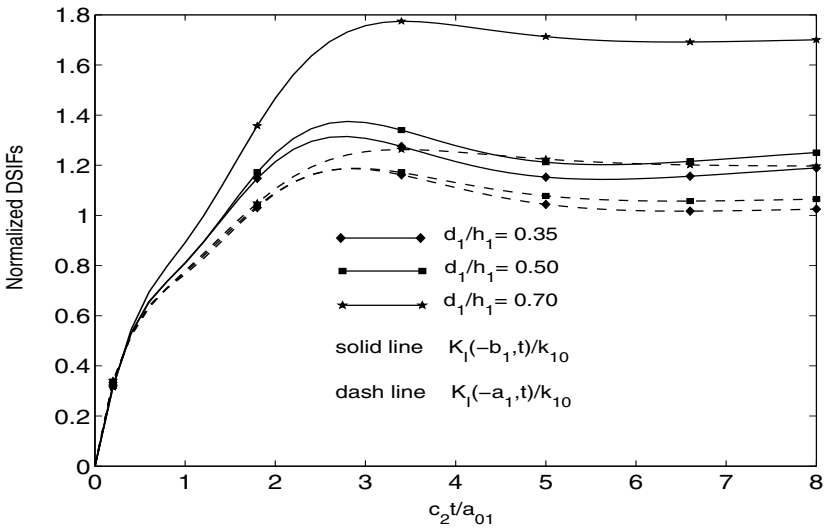

Figure 8: Influences of d_1 on DSIFs for two collinear cracks in different FGMs ($h_2/h_1 = 1, d_2/h_2 = 0.5, \beta_1 = -\ln 2.0, \beta_2 = \ln 2.0, a_{02}/h_2 = 0.2$)

values of $K_I(-b_1,t)/k_{10}$ are less than those of $K_I(-a_1,t)/k_{10}$ and when $\beta_1/\beta_2 < 0$, the reverse is true. Therefore, we conclude from Figs.6 and 7 that the peak and corresponding static values of the normalized DSIFs are larger for the crack tip lying in the relatively stiffer layer.

Fig.8 depicts the variations of the normalized DSIFs with d_1/h_1 when the two cracks both exist in the layered structure. It can be found that, both the peak and static values of $K_I(-b_1,t)/k_{10}$ are greater that those of $K_I(-a_1,t)/k_{10}$. The peak and corresponding static values of $K_I(-b_1,t)/k_{10}$ and $K_I(-a_1,t)/k_{10}$ increase with an increase of d_1/h_1, which shown that the crack tips are sensitive to the free surface of the coating when the crack center is far from the interface.

5.2 Bi-parameter exponential model

5.2.1 Internal cracks case

Figs.9 and 10 show the influence of nonhomogeneous parameter ratio β_1/β_2 on normalized DSIFs when $\alpha_1 = \alpha_2$=2.0 and $\alpha_1 = \alpha_2$=0.5, respectively. When $\alpha_1 = \alpha_2$=0.5, the peak and corresponding static values of $K_I(-b_1,t)/k_{10}$ are less than those of $K_I(-a_1,t)/k_{10}$. For $K_I(-b_1,t)/k_{10}$, it can be found that both the peak and static values increase with an increase of β_1/β_2. For $K_I(-a_1,t)/k_{10}$, however, the peak and the static values decrease with an increase of β_1/β_2. When $\alpha_1 = \alpha_2$=2.0

this feature is just opposite.

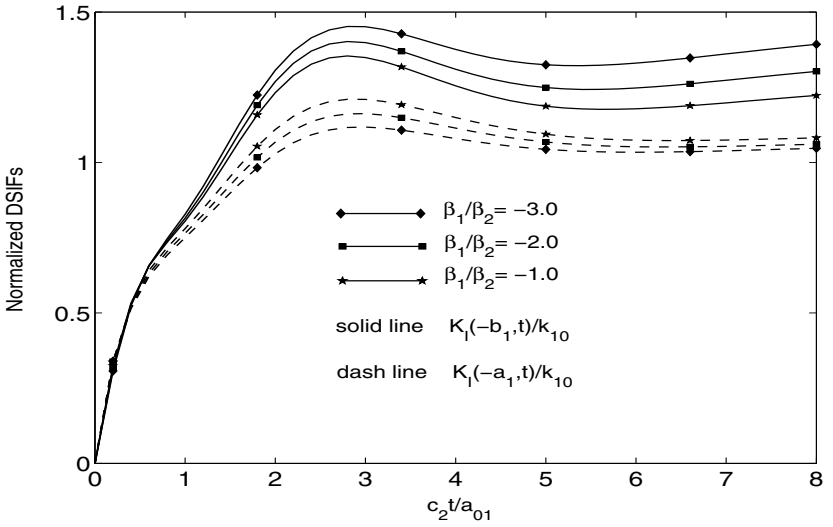

Figure 9: Influences of the ratio between the two nonhomogeneity parameters on the stress intensity factor of collinear cracks ($h_2/h_1 = 1, d_1/h_1 = 0.5, d_2/h_2 = 0.5, \beta_2 = \ln 2.0, a_{02}/h_2 = 0.2, \alpha_1 = \alpha_2 = 2.0$)

Figs.11 and 12 illustrate the influences of different thickness ratioes h_2/h_1 on normalized DSIFs when $\beta_1 = -\beta_2$. It can be found that the influence of h_2/h_1 on the peak value of DSIFs is not obvious. On the other hand, the static values of DSIFs decrease with an increase of h_2/h_1.

Assuming that ζ_2 is fixed, it can be found from Figs.13-15 that, when the nonhomogeneity parameter of FGM, β_1 and β_2, are fixed, the effect of another nonhomogeneity parameter of FGM, α_1, on the values of DSIFs of crack. When $\beta_1 = \beta_2$, for $K_I(-b_1,t)/k_{10}$, it can be seen that both the peak and static values decrease with the increasing of α_1. For $K_I(-a_1,t)/k_{10}$, however, the peak and the static values increase with the increasing of α_1. Furthermore, for $\alpha_1 < 1.0$ (such as α_1=0.1 or 0.5), the peak and static values of $K_I(-b_1,t)/k_{10}$ are greater than those of $K_I(-a_1,t)/k_{10}$. For $\alpha_1 > 1.0$ (such as α_1=2.0 or e), the peak and static values of $K_I(-b_1,t)/k_{10}$ are less than those of $K_I(-a_1,t)/k_{10}$. When $\beta_1 = -\beta_2$ just means the opposite case. From Fig.15, the peak value of $K_I(a_2,t)/k_{20}$ and $K_I(b_2,t)/k_{20}$ have no obvious variations with the increasing of α_1. However, the corresponding static values of $K_I(a_2,t)/k_{20}$ and $K_I(b_2,t)/k_{20}$ increase with an increase of α_1.

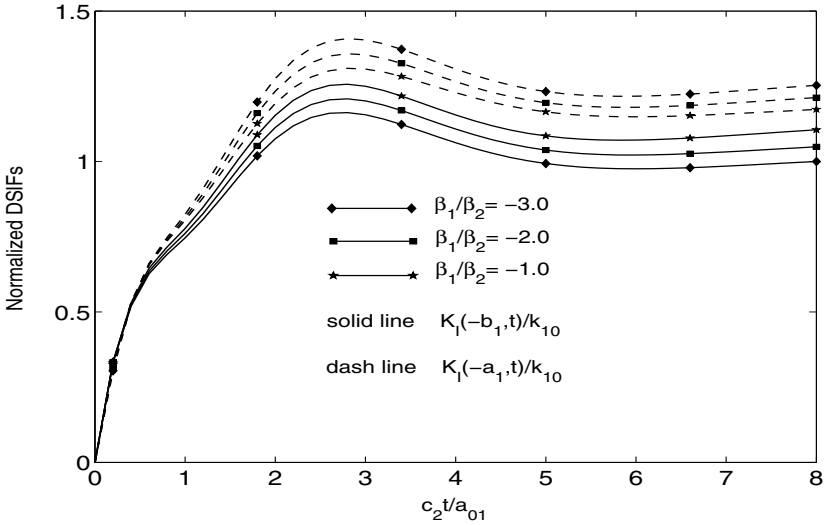

Figure 10: Influences of the ratio between the two nonhomogeneity parameters on the stress intensity factor of collinear cracks ($h_2/h_1 = 1, d_1/h_1 = 0.5, d_2/h_2 = 0.5, \beta_2 = \ln 2.0, a_{02}/h_2 = 0.2, \alpha_1 = \alpha_2 = 0.5$)

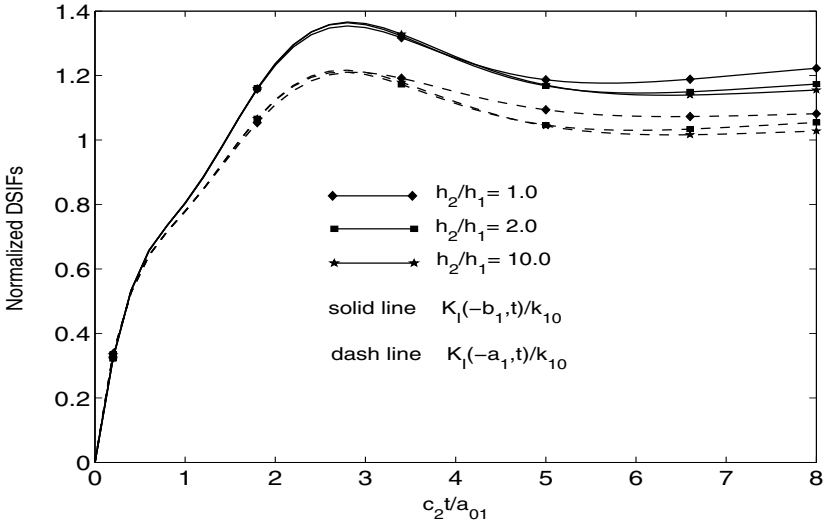

Figure 11: Influences of h_2/h_1 on DSIFs for collinear cracks ($d_1/h_1 = 0.5, d_2/h_2 = 0.5, \beta_1 = -\ln 2.0, \beta_2 = \ln 2.0, \alpha_1 = \alpha_2 = 2.0$)

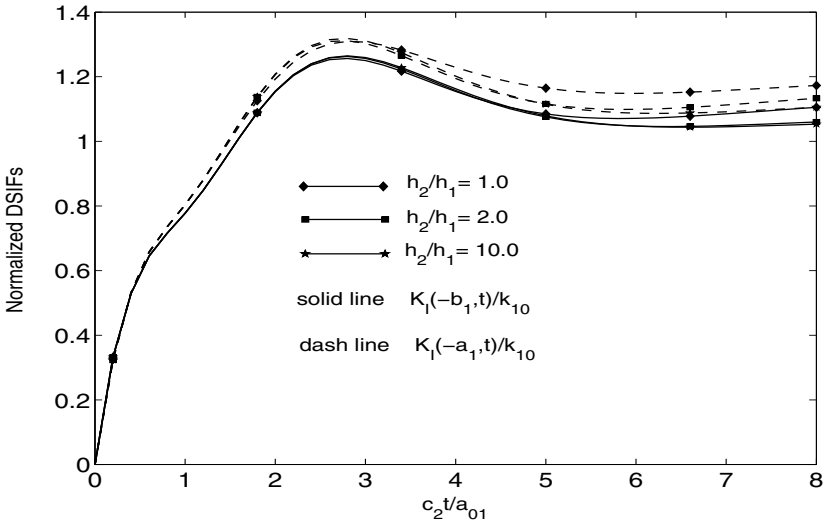

Figure 12: Influences of h_2/h_1 on DSIFs for collinear cracks ($d_1/h_1 = 0.5, d_2/h_2 = 0.5, \beta_1 = -\ln 2.0, \beta_2 = \ln 2.0, \alpha_1 = \alpha_2 = 0.5$)

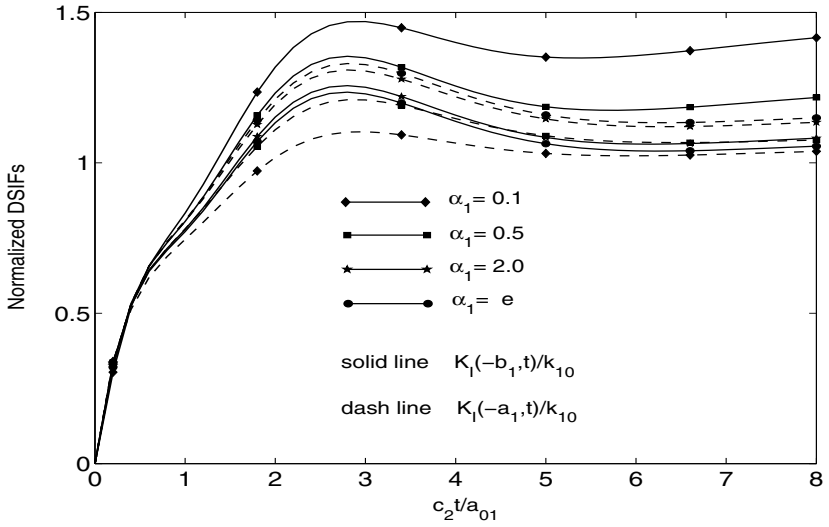

Figure 13: Influences of α_1 on DSIFs for collinear cracks ($h_2/h_1 = 1, d_1/h_1 = 0.5, d_2/h_2 = 0.5, \beta_1 = \beta_2 = \ln 2.0, \alpha_2 = e$)

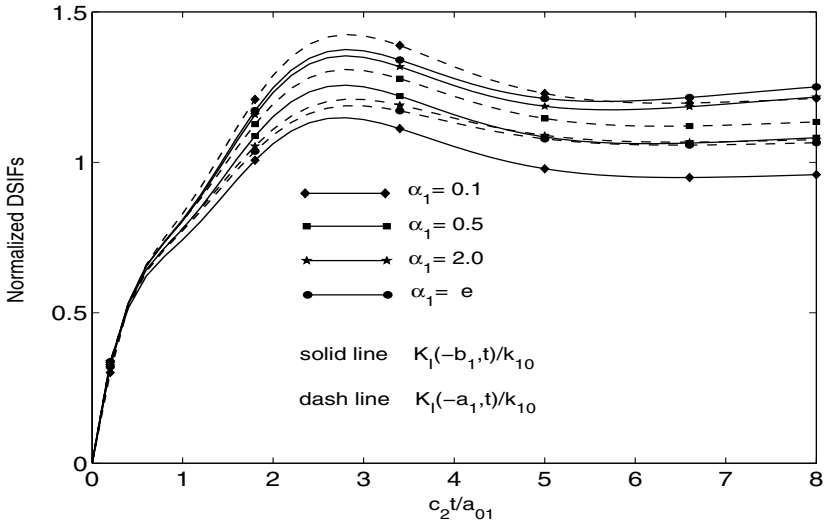

Figure 14: Influences of α_1 on DSIFs for collinear cracks ($h_2/h_1 = 1, d_1/h_1 = 0.5, d_2/h_2 = 0.5, \beta_1 = -\ln 2.0, \beta_2 = \ln 2.0, \alpha_2 = e$)

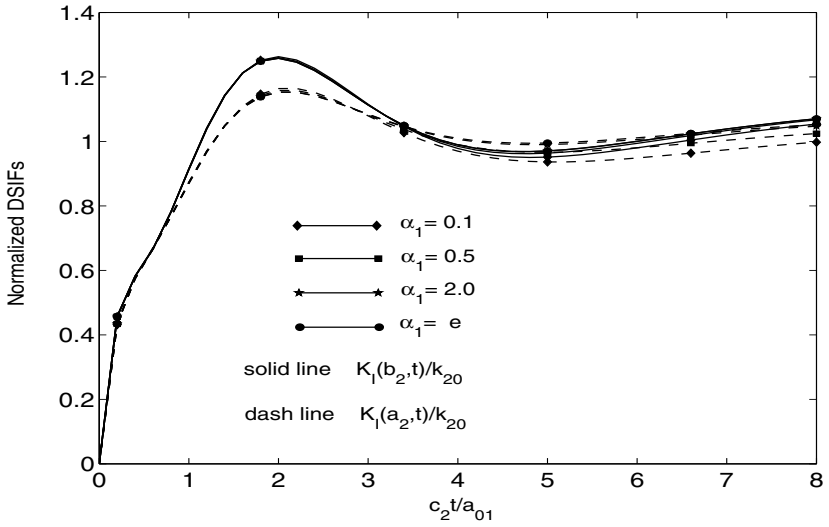

Figure 15: Influences of α_1 on DSIFs for collinear cracks ($h_2/h_1 = 1, d_1/h_1 = 0.5, d_2/h_2 = 0.5, \beta_1 = \beta_2 = \ln 2.0, \alpha_2 = e$)

5.2.2 Surface crack case

It can be found from Figs.16 and 17 that, when the non-homogeneity parameter of FGM_{II}, β_2, is fixed, with the nonhomogeneity parameter of FGM_I, $\beta_1 h_1$, increasing from ln0.1 to ln2.0, the peak values of normalized DSIFs increase for $\alpha_1 = \alpha_2$=2.0, and decrease for $\alpha_1 = \alpha_2$=0.5. By comparing the results for the edge crack problem with those for the internal crack problem, we found that: for the internal crack the DSIFs increase quickly with time and then keep approximately stable after reaching a peak, while the DSIFs for the edge crack also increase quickly with time but then exhibit a more obvious oscillation after reaching a peak. It is for the reason that the strip with an edge crack, compared with the structure with a central crack, loses symmetry, and the interaction between the waves and the finite boundaries would be stronger.

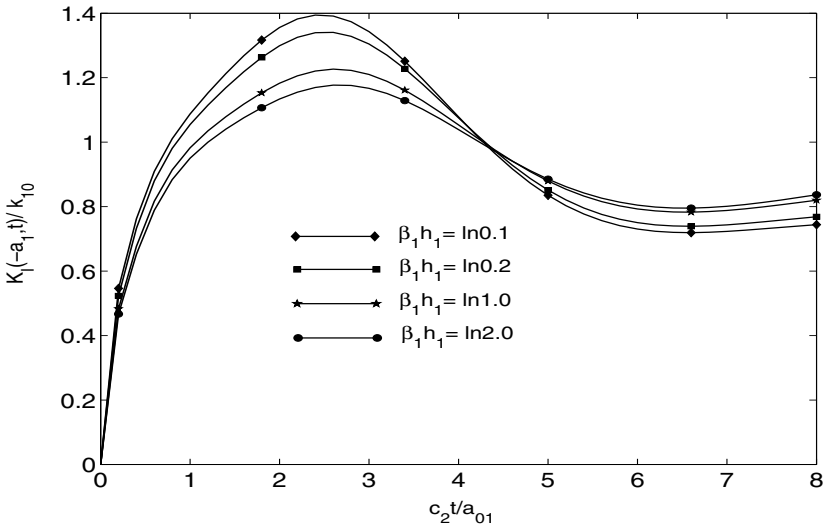

Figure 16: The effect of nonhomogeneity parameter on the DSIFs under the case of surface crack ($h_2/h_1 = 1, \beta_2 = \ln 2.0, a_{02} = 0.0, \alpha_1 = \alpha_2 = 0.5$)

By assuming that α_2 is fixed, Fig.18 shows the influence of α_1 on DSIFs when $\beta_1 = -\beta_2$. It can be seen that the peak of $K_I(-a_1,t)/k_{10}$ decrease with an increase of α_1. However, the corresponding static values of $K_I(-a_1,t)/k_{10}$ increase with an increase of of α_1.

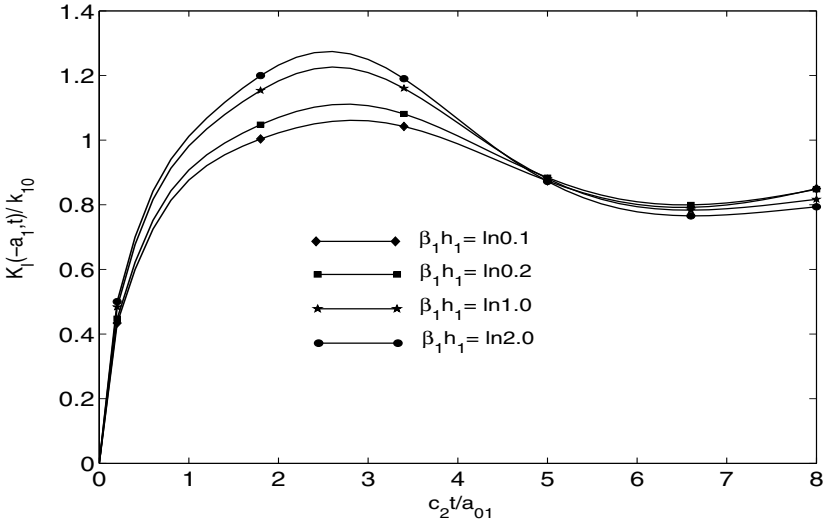

Figure 17: The effect of nonhomogeneity parameter on the DSIFs under the case of surface crack ($h_2/h_1 = 1, \beta_2 = \ln 2.0, a_{02} = 0.0, \alpha_1 = \alpha_2 = 2.0$)

5.2.3 Internal cracks crossing interface case

Figs.19 and 20 illustrates the variation of crack length a_{01}/h_1 on normalized DSIFs when $\alpha_1 = \alpha_2$=2.0 and $\alpha_1 = \alpha_2$=0.5, respectively. It can be found that both the peak and static values of DSIFs increase with the increasing of a_{01}/h_1 regardless of the variation of nonhomogeneous parameters. Meanwhile, it can be seen that, as the relative crack length a_{01}/h_1 increases, the peak value of DSIFs occurs at a later time. Undoubtedly, this is due to the interaction between the scattered waves from the crack and the reflected waves from the boundaries.

Figs.21 and 22 show the influence of $\beta_1 h_1$ on normalized DSIFs when $\alpha_1 = \alpha_2$=2.0 and $\alpha_1 = \alpha_2$=0.5, respectively. Similar to internal crack and edge crack problems, the variation of DSIFs is opposite with an changing of $\beta_1 h_1$ when $\alpha_1 = \alpha_2$=2.0 and $\alpha_1 = \alpha_2$=0.5, respectively.

Assuming that α_2 is fixed, Fig.23 show the influence of another nonhomogeneous parameter α_1 on DSIFs. It can be found that the peak value of $K_I(-b_1,t)/k_{10}$ increase with an increase of α_1.

6 Condusion

In this paper, the crack-tip fields in bonded functionally graded finite strips are studied. A new bi-parameter exponential function was introduced to simulate the

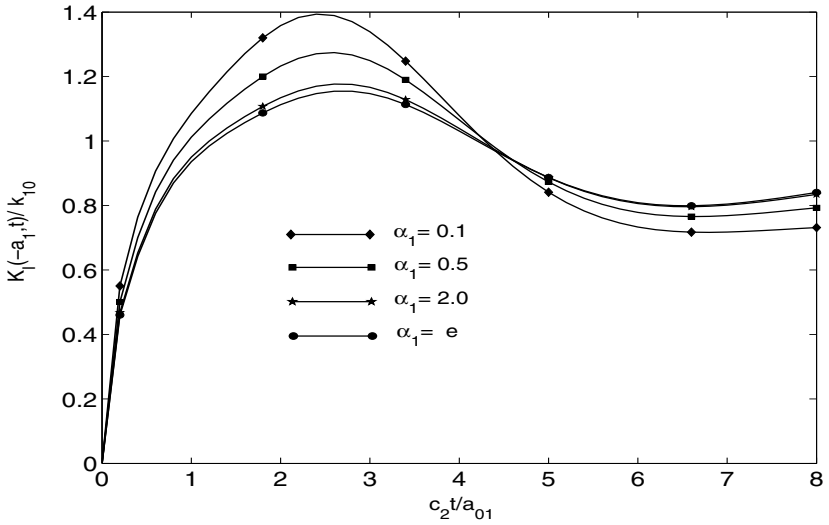

Figure 18: The effect of α_1 on the DSIFs under the case of surface crack ($h_2/h_1 = 1, \beta_1 = -\ln 2.0, \beta_2 = \ln 2.0, a_{02} = 0.0, \alpha_2 = e$)

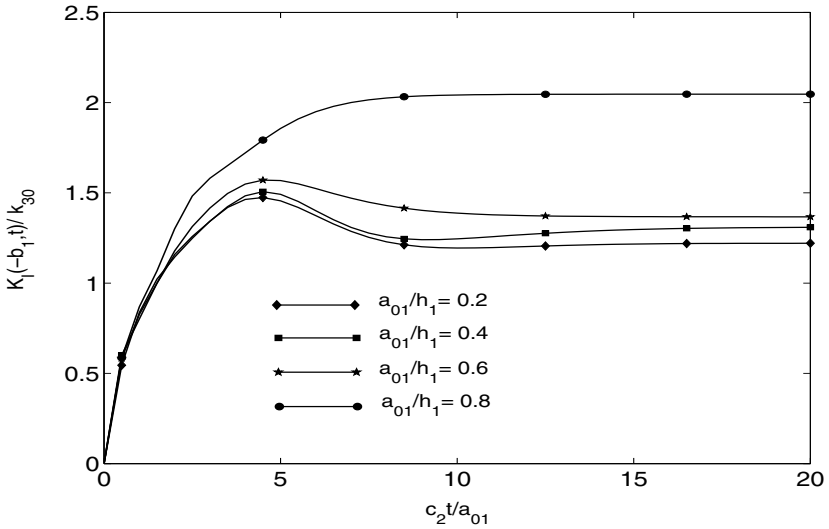

Figure 19: Influences of crack length on the DSIFs under the case of an internal crack crossing the interface ($h_2/h_1 = 1, \beta_1 = \beta_2 = \ln(1.455), \alpha_1 = \alpha_2 = 2.0$)

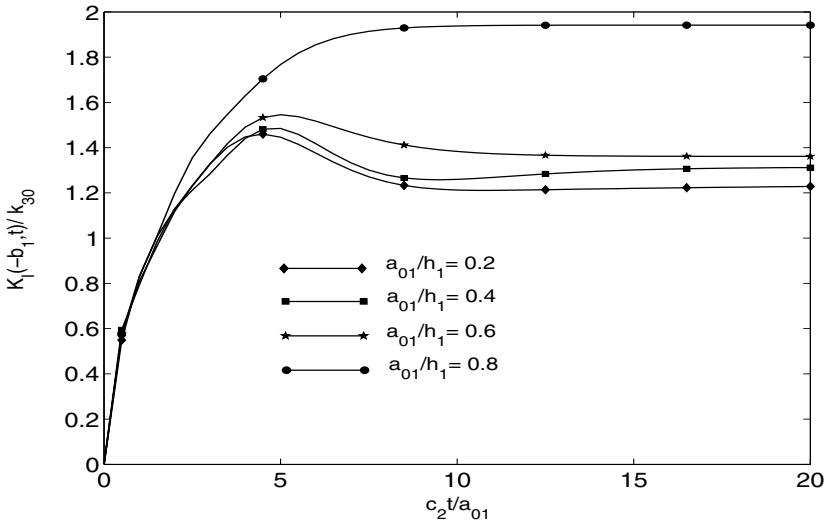

Figure 20: Influences of crack length on the DSIFs under the case of an internal crack crossing the interface ($h_2/h_1 = 1, \beta_1 = \beta_2 = \ln(1.455), \alpha_1 = \alpha_2 = 0.5$)

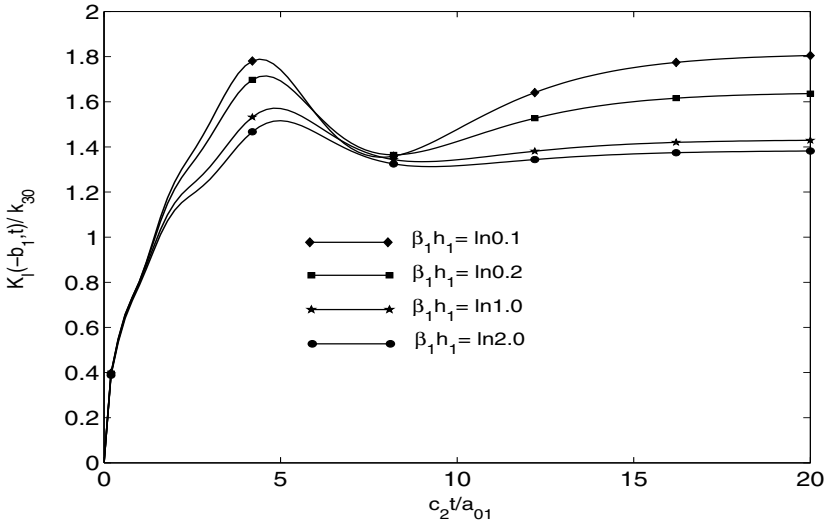

Figure 21: Influences of nonhomogeneity parameter on the DSIFs under the case of an internal crack crossing the interface ($h_2/h_1 = 1, \beta_2 = \ln 0.2, \alpha_1 = \alpha_2 = 2.0$)

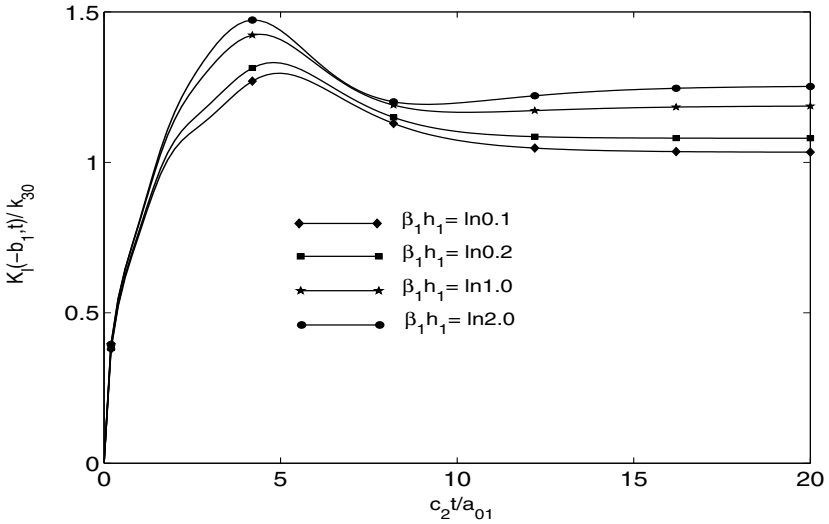

Figure 22: Influences of nonhomogeneity parameter on the DSIFs under the case of an internal crack crossing the interface ($h_2/h_1 = 1, \beta_2 = \ln 0.2, \alpha_1 = \alpha_2 = 0.5$)

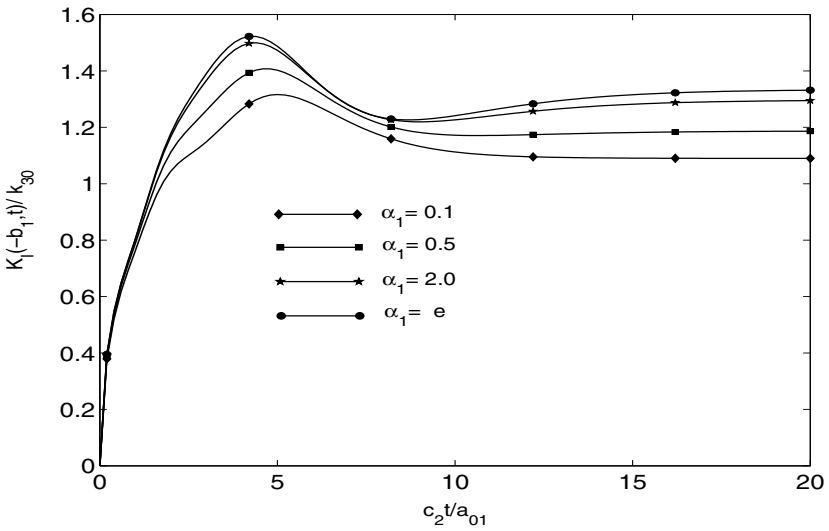

Figure 23: Influences of nonhomogeneity parameter on the DSIFs under the case of an internal crack crossing the interface ($h_2/h_1 = 1, \beta_1 = -\ln 2.0, \beta_2 = \ln 2.0, \alpha_2 = e$)

continuous variation of material properties. The singular integral equation for solving the problem and the corresponding asymptotic expression of the singular kernel are obtained. Various internal cracks and edge crack and crack crossing the interface configurations are investigated, respectively. The following conclusions could be made

- The asymptotic stress field near the tip of a crack crossing the interface was obtained which has the conventional square root singularity and the same angular distribution structure as that of mode I crack in elastic homogeneous material.
- Consider the single crack and two collinear cracks problem. As the ligament between the crack shortens in length, the effect is more pronounced on DSIFs.
- Compared to internal crack, for an edge crack, it is observed that the curves of DSIFs oscillate more obviously with the increasing of nonhomogeneity constant, and the occurring time for the peak value decreases with the increasing of nonhomogeneity constant.
- In the case of $\alpha_1 > 1$ and $\alpha_2 > 1$ (such as $\alpha_1 = \alpha_2$=2.0), the variation of both peak and static values of DSIFs with changing of nonhomogeneous parameters is opposite to the case of $\alpha_1 < 1$ and $\alpha_2 < 1$ (such as $\alpha_1 = \alpha_2$=0.5).
- To increase the rigidity of the FGM strip where the crack is located will increase the DSIFs. However, when the material in one side of the interface is more rigid, the DSIFs of the interface-perpendicular crack in the other side will be reduced.

Acknowledgement: This work was supported by the National Natural Science Foundation of China (10962008) and the Ningxia University Science Foundation ((E)ndzr09-8, ZR200805).

Appendix A

The expressions of $m_{kj}(s,p)$, n_{kj}, $q_{kj}(s,p)$ and p_{kj} $(k = 1,2, j = 1-4)$ are given by

$$n_{kj}(s,p) = \pm 1/2 \sqrt{4\Lambda_{11}{}^2 + \Lambda_{12}{}^2 \pm 4\sqrt{\Lambda_{11}{}^2\Lambda_{12}{}^2 + \frac{p^4\rho_0}{\mu_0{}^2(\kappa+1)^2}}}, \tag{A1}$$

$$m_{kj}(s,p)=\frac{(\kappa-1)\mu_0 s(s+i\beta_k\ln\alpha_k)-mu_0(\kappa+1)n_{kj}^2+(\kappa-1)p^2\rho_0}{\mu_0(\beta_k\ln\alpha_k(\kappa-1)-2is)n_{kj}}, \tag{A2}$$

$$p_{kj}(\alpha,p)=-1/2\,\beta_k\ln\alpha_k\pm 1/2\sqrt{4\,\alpha^2+(\beta_k\ln\alpha_k)^2+\frac{4\kappa p^2\rho_0\pm 4\Omega_k}{\mu_0(\kappa+1)}}, \tag{A3}$$

$$q_{kj}(\alpha,p)=\frac{-(\kappa+1)\mu_0\alpha^2+(\kappa-1)(\beta_k\ln\alpha_k\mu_0 p_{kj}+\mu_0 p_{kj}^2-p^2\rho_0)}{\mu_0((\kappa-1)\beta_k\ln\alpha_k+2p_{kj})\alpha}, \tag{A4}$$

$$\Omega_k=\sqrt{\alpha^2(\beta_k\ln\alpha_k)^2\mu_0{}^2\kappa^2-2\,\alpha^2(\beta_k\ln\alpha_k)^2\mu_0{}^2\kappa-3\,\alpha^2(\beta_k\ln\alpha_k)^2\mu_0{}^2+p^4\rho_0{}^2}. \tag{A5}$$

The expressions of c_{kj}, d_{kj}, and $e_{kj}(k=1,2,j=1-4)$ are given by

$$c_{1j}=\frac{\mu_0}{\kappa-1}((3-\kappa)n_{1j}-(\kappa+1)m_{1j}is),\quad c_{2j}=\frac{\mu_0}{\kappa-1}((3-\kappa)n_{2j}-(\kappa+1)m_{2j}is), \tag{A6}$$

$$c_{3j}=\frac{\mu_0}{\kappa-1}((3-\kappa)\alpha+(\kappa+1)q_{1j}p_{1j}),\quad c_{4j}=\frac{\mu_0}{\kappa-1}((3-\kappa)\alpha+(\kappa+1)q_{2j}p_{2j}), \tag{A7}$$

$$d_{1j}=\frac{\mu_0}{\kappa-1}((1+\kappa)n_{1j}-(3-\kappa)m_{1j}is),\quad d_{2j}=\frac{\mu_0}{\kappa-1}((1+\kappa)n_{2j}-(3-\kappa)m_{2j}is), \tag{A8}$$

$$d_{3j}=\frac{\mu_0}{\kappa-1}((1+\kappa)\alpha+(3-\kappa)q_{1j}p_{1j}),\quad d_{4j}=\frac{\mu_0}{\kappa-1}((1+\kappa)\alpha+(3-\kappa)q_{2j}p_{2j}), \tag{A9}$$

$$\begin{aligned} &e_{1j}=\mu_0(m_{1j}n_{1j}-is),\quad e_{2j}=\mu_0(m_{2j}n_{2j}-is),\\ &e_{3j}=\mu_0(p_{1j}-q_{1j}\alpha),\quad e_{4j}=\mu_0(p_{2j}-q_{2j}\alpha). \end{aligned} \tag{A10}$$

Appendix B

$\widehat{C}_j$ and $\widehat{D}_j$ $(j=1-8)$ can be given by

$$\widehat{C}_j(t_1,\alpha,p)=\sum_{k=1}^{8}b_{jk}(\alpha,p)\widehat{R}_{k1}(\alpha,p),\quad j=1-8, \tag{B1}$$

$$\widehat{D}_j(t_2,\alpha,p)=\sum_{k=1}^{8} b_{jk}(\alpha,p)\widehat{R}_{k2}(\alpha,p),\quad j=1-8, \tag{B2}$$

where

$$\widehat{R}_{11}(\alpha,p)=R_{11}(\alpha,p)e^{-p_{13}(t_1+h_1)}+R_{12}(\alpha,p)e^{-p_{14}(t_1+h_1)}+R_{13}(\alpha,p), \tag{B3}$$

$$\widehat{R}_{21}(\alpha,p)=R_{21}(\alpha,p)e^{-p_{13}(t_1+h_1)}+R_{22}(\alpha,p)e^{-p_{14}(t_1+h_1)}+R_{23}(\alpha,p), \tag{B4}$$

$$\widehat{R}_{12}(\alpha,p)=0,\quad \widehat{R}_{22}(\alpha,p)=0, \tag{B5}$$

$$\widehat{R}_{31}(\alpha,p)=R_{311}(\alpha,p)e^{-p_{11}t_1}+R_{312}(\alpha,p)e^{-p_{12}t_1}+R_{313}(\alpha,p), \tag{B6}$$

$$\widehat{R}_{32}(\alpha,p)=R_{321}(\alpha,p)e^{-p_{23}t_2}+R_{322}(\alpha,p)e^{-p_{24}t_2}+R_{323}(\alpha,p), \tag{B7}$$

$$\widehat{R}_{41}(\alpha,p)=R_{411}(\alpha,p)e^{-p_{11}t_1}+R_{412}(\alpha,p)e^{-p_{12}t_1}+R_{413}(\alpha,p), \tag{B8}$$

$$\widehat{R}_{42}(\alpha,p)=R_{421}(\alpha,p)e^{-p_{23}t_2}+R_{422}(\alpha,p)e^{-p_{24}t_2}+R_{423}(\alpha,p), \tag{B9}$$

$$\widehat{R}_{51}(\alpha,p)=0,\quad \widehat{R}_{61}(\alpha,p)=0, \tag{B10}$$

$$\widehat{R}_{52}(\alpha,p)=R_{51}(\alpha,p)e^{-p_{21}(t_2-h_2)}+R_{52}(\alpha,p)e^{-p_{22}(t_2-h_2)}+R_{53}(\alpha,p), \tag{B11}$$

$$\widehat{R}_{62}(\alpha,p)=R_{61}(\alpha,p)e^{-p_{21}(t_2-h_2)}+R_{62}(\alpha,p)e^{-p_{22}(t_2-h_2)}+R_{63}(\alpha,p), \tag{B12}$$

$$\widehat{R}_{71}(\alpha,p)=R_{711}(\alpha,p)e^{-p_{11}t_1}+R_{712}(\alpha,p)e^{-p_{12}t_1}+R_{713}(\alpha,p), \tag{B13}$$

$$\widehat{R}_{72}(\alpha,p)=R_{721}(\alpha,p)e^{-p_{23}t_2}+R_{722}(\alpha,p)e^{-p_{24}t_2}+R_{723}(\alpha,p), \tag{B14}$$

$$\widehat{R}_{81}(\alpha,p)=R_{811}(\alpha,p)e^{-p_{11}t_1}+R_{812}(\alpha,p)e^{-p_{12}t_1}+R_{813}(\alpha,p), \tag{B15}$$

$$\widehat{R}_{82}(\alpha,p)=R_{821}(\alpha,p)e^{-p_{23}t_2}+R_{822}(\alpha,p)e^{-p_{24}t_2}+R_{823}(\alpha,p), \tag{B16}$$

$$R_{11}(\alpha,p)=\frac{p_{13}{}^2\mu_0\left(8\alpha^2\mu_0-(\kappa-3)p^2\rho_0\right)-(\kappa-3)p^2\rho_0\left(\mu_0\beta_1\ln\alpha_1 p_{13}-\alpha^2\mu_0-p^2\rho_0\right)}{(1+\kappa)\mu_0 p_{13}(p_{13}-p_{11})(p_{13}-p_{12})(p_{13}-p_{14})}, \tag{B17}$$

$$R_{12}(\alpha,p)=\frac{p_{14}{}^2\mu_0\left(8\alpha^2\mu_0-(\kappa-3)p^2\rho_0\right)-(\kappa-3)p^2\rho_0\left(\mu_0\beta_1\ln\alpha_1 p_{14}-\alpha^2\mu_0-p^2\rho_0\right)}{(1+\kappa)\mu_0 p_{14}(p_{14}-p_{11})(p_{14}-p_{12})(p_{14}-p_{13})}, \tag{B18}$$

$$R_{13}(\alpha,p)=\frac{(\kappa-3)p^2\rho_0\left(\alpha^2\mu_0+p^2\rho_0\right)}{2(1+\kappa)\mu_0 p_{11}p_{12}p_{13}p_{14}}, \tag{B19}$$

$$R_{21}(\alpha,p)=-\frac{\alpha\left(8\mu_0{p_{13}}^3+8\beta_1\ln\alpha_1\mu_0{p_{13}}^2-4p^2\rho_0p_{13}+(\kappa-3)p^2\beta_1\ln\alpha_1\rho_0\right)}{(1+\kappa)p_{13}(p_{13}-p_{11})(p_{13}-p_{12})(p_{13}-p_{14})}, \tag{B20}$$

$$R_{22}(\alpha,p)=-\frac{\alpha\left(8\mu_0{p_{14}}^3+8\beta_1\ln\alpha_1\mu_0{p_{14}}^2-4p^2\rho_0p_{14}+(\kappa-3)p^2\beta_1\ln\alpha_1\rho_0\right)}{(1+\kappa)p_{14}(p_{14}-p_{11})(p_{14}-p_{12})(p_{14}-p_{13})}, \tag{B21}$$

$$R_{23}(\alpha,p)=-\frac{\alpha(\kappa-3)p^2\rho_0\beta_1\ln\alpha_1}{2(1+\kappa)p_{11}p_{12}p_{13}p_{14}}, \tag{B22}$$

$$R_{311}(\alpha,p)= -\frac{{p_{11}}^2\mu_0\left(8\alpha^2\mu_0-(\kappa-3)p^2\rho_0\right)-(\kappa-3)p^2\rho_0\left(\mu_0\beta_1\ln\alpha_1p_{11}-\alpha^2\mu_0-p^2\rho_0\right)}{(1+\kappa)\mu_0p_{11}(p_{11}-p_{12})(p_{11}-p_{13})(p_{11}-p_{14})}, \tag{B23}$$

$$R_{312}(\alpha,p)= -\frac{{p_{12}}^2\mu_0\left(8\alpha^2\mu_0-(\kappa-3)p^2\rho_0\right)-(\kappa-3)p^2\rho_0\left(\mu_0\beta_1\ln\alpha_1p_{12}-\alpha^2\mu_0-p^2\rho_0\right)}{(1+\kappa)\mu_0p_{12}(p_{12}-p_{11})(p_{12}-p_{13})(p_{12}-p_{14})}, \tag{B24}$$

$$R_{313}(\alpha,p)=-\frac{(\kappa-3)p^2\rho_0\left(\alpha^2\mu_0+p^2\rho_0\right)}{2(1+\kappa)\mu_0p_{11}p_{12}p_{13}p_{14}}, \tag{B25}$$

$$R_{321}(\alpha,p)= \frac{{p_{23}}^2\mu_0\left(-8\alpha^2\mu_0+(\kappa-3)p^2\rho_0\right)-(\kappa-3)p^2\rho_0\left(-\mu_0\beta_2\ln\alpha_2p_{23}+\alpha^2\mu_0+p^2\rho_0\right)}{(1+\kappa)\mu_0p_{23}(p_{23}-p_{21})(p_{23}-p_{22})(p_{23}-p_{24})}, \tag{B26}$$

$$R_{322}(\alpha,p)= \frac{{p_{24}}^2\mu_0\left(-8\alpha^2\mu_0+(\kappa-3)p^2\rho_0\right)-(\kappa-3)p^2\rho_0\left(-\mu_0\beta_2\ln\alpha_2p_{24}+\alpha^2\mu_0+p^2\rho_0\right)}{(1+\kappa)\mu_0p_{24}(p_{24}-p_{21})(p_{24}-p_{22})(p_{24}-p_{23})}, \tag{B27}$$

$$R_{323}(\alpha,p)=-\frac{(\kappa-3)p^2\rho_0\left(\alpha^2\mu_0+p^2\rho_0\right)}{2(1+\kappa)\mu_0p_{21}p_{22}p_{23}p_{24}}, \tag{B28}$$

$$R_{411}(\alpha,p)=\frac{\alpha\left(8\,\mu_0 {p_{11}}^3+8\,\beta_1\ln\alpha_1\mu_0 {p_{11}}^2-4\,p^2\rho_0 p_{11}+(\kappa-3)\,p^2\beta_1\ln\alpha_1\rho_0\right)}{(1+\kappa)\,p_{11}\,(p_{11}-p_{12})\,(p_{11}-p_{13})\,(p_{11}-p_{14})},\tag{B29}$$

$$R_{412}(\alpha,p)=\frac{\alpha\left(8\,\mu_0 {p_{12}}^3+8\,\beta_1\ln\alpha_1\mu_0 {p_{12}}^2-4\,p^2\rho_0 p_{12}+(\kappa-3)\,p^2\beta_1\ln\alpha_1\rho_0\right)}{(1+\kappa)\,p_{12}\,(p_{12}-p_{11})\,(p_{12}-p_{13})\,(p_{12}-p_{14})},\tag{B30}$$

$$R_{413}(\alpha,p)=\frac{\alpha\,(\kappa-3)\,p^2\rho_0\beta_1\ln\alpha_1}{2\,(1+\kappa)\,p_{11}p_{12}p_{13}p_{14}},\tag{B31}$$

$$R_{421}(\alpha,p)=\frac{\alpha\left(8\,\mu_0 {p_{23}}^3+8\,\beta_2\ln\alpha_2\mu_0 {p_{23}}^2-4\,p^2\rho_0 p_{23}+(\kappa-3)\,p^2\beta_2\ln\alpha_2\rho_0\right)}{(1+\kappa)\,p_{23}\,(p_{23}-p_{21})\,(p_{23}-p_{22})\,(p_{23}-p_{24})},\tag{B32}$$

$$R_{422}(\alpha,p)=\frac{\alpha\left(8\,\mu_0 {p_{24}}^3+8\,\beta_2\ln\alpha_2\mu_0 {p_{24}}^2-4\,p^2\rho_0 p_{24}+(\kappa-3)\,p^2\beta_2\ln\alpha_2\rho_0\right)}{(1+\kappa)\,p_{24}\,(p_{24}-p_{21})\,(p_{24}-p_{22})\,(p_{24}-p_{23})},\tag{B33}$$

$$R_{423}(\alpha,p)=\frac{\alpha\,(\kappa-3)\,p^2\rho_0\beta_2\ln\alpha_2}{2\,(1+\kappa)\,p_{21}p_{22}p_{23}p_{24}},\tag{B34}$$

$$R_{51}(\alpha,p)=\frac{{p_{21}}^2\mu_0\left(8\,\alpha^2\mu_0-(\kappa-3)\,p^2\rho_0\right)+(\kappa-3)\,p^2\rho_0\left(-\mu_0\beta_2\ln\alpha_2 p_{21}+\alpha^2\mu_0+p^2\rho_0\right)}{(1+\kappa)\,\mu_0 p_{21}\,(p_{21}-p_{22})\,(p_{21}-p_{23})\,(p_{21}-p_{24})},\tag{B35}$$

$$R_{52}(\alpha,p)=\frac{{p_{22}}^2\mu_0\left(8\,\alpha^2\mu_0-(\kappa-3)\,p^2\rho_0\right)+(\kappa-3)\,p^2\rho_0\left(-\mu_0\beta_2\ln\alpha_2 p_{22}+\alpha^2\mu_0+p^2\rho_0\right)}{(1+\kappa)\,\mu_0 p_{22}\,(p_{22}-p_{21})\,(p_{22}-p_{23})\,(p_{22}-p_{24})},\tag{B36}$$

$$R_{53}(\alpha,p)=\frac{(\kappa-3)\,p^2\rho_0\left(\alpha^2\mu_0+p^2\rho_0\right)}{2\,(1+\kappa)\,\mu_0 p_{21}p_{22}p_{23}p_{24}},\tag{B37}$$

$$R_{61}(\alpha,p)= -\frac{\alpha\left(8\mu_0 {p_{21}}^3+8\beta_2\ln\alpha_2\mu_0 {p_{21}}^2-4p^2\rho_0 p_{21}+(\kappa-3)p^2\beta_2\ln\alpha_2\rho_0\right)}{(1+\kappa)p_{21}(p_{21}-p_{22})(p_{21}-p_{23})(p_{21}-p_{24})}, \quad \text{(B38)}$$

$$R_{62}(\alpha,p)= -\frac{\alpha\left(8\mu_0 {p_{22}}^3+8\beta_2\ln\alpha_2\mu_0 {p_{22}}^2-4p^2\rho_0 p_{22}+(\kappa-3)p^2\beta_2\ln\alpha_2\rho_0\right)}{(1+\kappa)p_{22}(p_{22}-p_{21})(p_{22}-p_{23})(p_{22}-p_{24})}, \quad \text{(B39)}$$

$$R_{63}(\alpha,p)= -\frac{\alpha(\kappa-3)p^2\rho_0\beta_2\ln\alpha_2}{2(1+\kappa)p_{21}p_{22}p_{23}p_{24}}, \quad \text{(B40)}$$

$$R_{711}(\alpha,p)= -[(\kappa-3)p^2\beta_1\ln\alpha_1\rho_0+(\alpha^2(1+\kappa)\mu_0 -(\kappa-3)(\mu_0(\beta_1\ln\alpha_1)^2-p^2\rho_0))p_{11}-(\kappa-3)\mu_0 {p_{11}}^2(2\beta_1\ln\alpha_1+p_{11})] /[(1+\kappa)\mu_0 p_{11}(p_{11}-p_{12})(p_{11}-p_{13})(p_{11}-p_{14})], \quad \text{(B41)}$$

$$R_{712}(\alpha,p)= -[(\kappa-3)p^2\beta_1\ln\alpha_1\rho_0+(\alpha^2(1+\kappa)\mu_0 -(\kappa-3)(\mu_0(\beta_1\ln\alpha_1)^2-p^2\rho_0))p_{12}-(\kappa-3)\mu_0 {p_{12}}^2(2\beta_1\ln\alpha_1+p_{12})]/ [(1+\kappa)\mu_0 p_{12}(p_{12}-p_{11})(p_{12}-p_{13})(p_{12}-p_{14})], \quad \text{(B42)}$$

$$R_{713}(\alpha,p)= -\frac{(\kappa-3)p^2\beta_1\ln\alpha_1\rho_0}{2(1+\kappa)\mu_0 p_{11}p_{12}p_{13}p_{14}}, \quad \text{(B43)}$$

$$R_{721}(\alpha,p)= -[(\kappa-3)p^2\beta_2\ln\alpha_2\rho_0-(\alpha^2(1+\kappa)\mu_0 -(\kappa-3)(\mu_0(\beta_2\ln\alpha_2)^2-p^2\rho_0))p_{23}+(\kappa-3)\mu_0 {p_{23}}^2(2\beta_2\ln\alpha_2+p_{23})]/ [(1+\kappa)\mu_0 p_{23}(p_{23}-p_{21})(p_{23}-p_{22})(p_{23}-p_{24})], \quad \text{(B44)}$$

$$R_{722}(\alpha,p)= [-(\kappa-3)p^2\beta_2\ln\alpha_2\rho_0-(\alpha^2(1+\kappa)\mu_0 -(\kappa-3)(\mu_0(\beta_2\ln\alpha_2)^2-p^2\rho_0))p_{24}+(\kappa-3)\mu_0 {p_{24}}^2(2\beta_2\ln\alpha_2+p_{24})] [(1+\kappa)\mu_0 p_{24}(p_{24}-p_{21})(p_{24}-p_{22})(p_{24}-p_{23})], \quad \text{(B45)}$$

$$R_{723}(\alpha,p)= -\frac{(\kappa-3)p^2\beta_2\ln\alpha_2\rho_0}{2(1+\kappa)\mu_0 p_{21}p_{22}p_{23}p_{24}}, \quad \text{(B46)}$$

$$R_{811}(\alpha,p) = -[((\alpha^2\mu_0 + p^2\rho_0)(1+\kappa) - (\kappa-3)\mu_0(\beta_1 \ln\alpha_1)^2 - 2p_{11}(1+\kappa)\mu_0\beta_1 \ln\alpha_1 - (\kappa+5)\mu_0 {p_{11}}^2)\alpha]/[(1+\kappa)\mu_0 p_{11}(p_{11}-p_{12})(p_{11}-p_{13})(p_{11}-p_{14})], \quad \text{(B47)}$$

$$R_{812}(\alpha,p) = -[((\alpha^2\mu_0 + p^2\rho_0)(1+\kappa) - (\kappa-3)\mu_0(\beta_1 \ln\alpha_1)^2 - 2p_{12}(1+\kappa)\mu_0\beta_1 \ln\alpha_1 - (\kappa+5)\mu_0 {p_{12}}^2)\alpha]/[(1+\kappa)\mu_0 p_{12}(p_{12}-p_{11})(p_{12}-p_{13})(p_{12}-p_{14})], \quad \text{(B48)}$$

$$R_{813}(\alpha,p) = -\frac{((\alpha^2\mu_0 + p^2\rho_0)(1+\kappa) - (\kappa-3)\mu_0(\beta_1 \ln\alpha_1)^2)\alpha}{2(1+\kappa)\mu_0 p_{11}p_{12}p_{13}p_{14}}, \quad \text{(B49)}$$

$$R_{821}(\alpha,p) = [(-(\alpha^2\mu_0 + p^2\rho_0)(1+\kappa) + (\kappa-3)\mu_0(\beta_2 \ln\alpha_2)^2 + 2p_{23}(1+\kappa)\mu_0\beta_2 \ln\alpha_2 + (\kappa+5)\mu_0 {p_{23}}^2)\alpha]/[(1+\kappa)\mu_0 p_{23}(p_{23}-p_{21})(p_{23}-p_{22})(p_{23}-p_{24})], \quad \text{(B50)}$$

$$R_{822}(\alpha,p) = [(-(\alpha^2\mu_0 + p^2\rho_0)(1+\kappa) + (\kappa-3)\mu_0(\beta_2 \ln\alpha_2)^2 + 2p_{24}(1+\kappa)\mu_0\beta_2 \ln\alpha_2 + (\kappa+5)\mu_0 {p_{24}}^2)\alpha]/[(1+\kappa)\mu_0 p_{24}(p_{24}-p_{21})(p_{24}-p_{22})(p_{24}-p_{23})], \quad \text{(B51)}$$

$$R_{823}(\alpha,p) = \frac{(-(\alpha^2\mu_0 + p^2\rho_0)(1+\kappa) + (\kappa-3)\mu_0(\beta_2 \ln\alpha_2)^2)\alpha}{2(1+\kappa)\mu_0 p_{21}p_{22}p_{23}p_{24}}. \quad \text{(B52)}$$

The matrix (b_{jk}) is the inverse of (a_{jk}). The non-zero vectors of (a_{jk}) are expressed as

$$a_{1j} = c_{3j}\exp(m_{1j}h_1), \quad a_{2j} = e_{3j}\exp(m_{1j}h_1), \quad j = 1-4, \quad \text{(B53)}$$

$$a_{3j} = c_{3j}, \quad a_{4j} = e_{3j}, \quad j = 1-4, \quad a_{3j} = -c_{4j}, \quad a_{4j} = -e_{4j}, \quad j = 5-8, \quad \text{(B54)}$$

$$a_{5j} = c_{4j}\exp(-m_{2j}h_2), \quad a_{6j} = e_{4j}\exp(-m_{2j}h_1), \quad j = 5-8, \quad \text{(B55)}$$

$$a_{7j} = G_{1j}, \quad a_{8j} = 1, \quad j = 1-4, \quad a_{7j} = -G_{2j}, \quad a_{8j} = -1, \quad j = 5-8. \quad \text{(B56)}$$

Appendix C

The functions $k_{11}(y,s,p), k_{12}(\alpha,x_1,t_1,p), k_{13}(\alpha,x_1,t_2,p), k_{21}(y,s,p), k_{22}(\alpha,x_2,t_1,p)$ and $k_{23}(\alpha,x_2,t_2,p)$ are

$$\begin{aligned} k_{11}(y,s,p) &= d_{11}f_{11}\exp(n_{11}y) + d_{12}f_{12}\exp(n_{12}y), \\ k_{12}(\alpha,x_1,t_1,p) &= \sum_{j=1}^{4}\sum_{k=1}^{8} d_{3j}b_{jk}\widehat{R}_{k1}\exp(p_{1j}x_1), \end{aligned} \quad \text{(C1)}$$

$$k_{13}(\alpha,x_1,t_1,p)=\sum_{j=1}^{4}\sum_{k=1}^{8}d_{3j}b_{jk}\widehat{R}_{k2}\exp(p_{1j}x_1),$$
$$k_{21}(y,s,p)=d_{21}f_{21}\exp(n_{21}y)+d_{22}f_{22}\exp(n_{22}y), \tag{C2}$$

$$k_{22}(\alpha,x_2,t_2,p)=\sum_{j=1}^{4}\sum_{k=1}^{8}d_{4j}b_{jk}\widehat{R}_{k1}\exp(p_{2j}x_2),$$
$$k_{23}(\alpha,x_2,t_2,p)=\sum_{j=1}^{4}\sum_{k=1}^{8}d_{4j}b_{jk}\widehat{R}_{k2}\exp(p_{2j}x_2), \tag{C3}$$

The kernel functions $H_{ij}(i=1,2,j=1,2)$ can be given by

$$H_{11}(x_1,t_1,p)=\frac{1+\kappa}{8\mu_0}\left\{\int_0^A(k_{11}+k_{11c})\cos[s(t_1-x_1)]ds\right.$$
$$+\int_A^\infty(k_{11}+k_{11c}-\frac{4\beta_1\ln\alpha_1\mu_0}{s(1+\kappa)})\cos[s(t_1-x_1)]ds$$
$$\left.+\int_0^\infty(k_{11}-k_{11c}+\frac{8i\mu_0}{1+\kappa})i\sin[s(t_1-x_1)]ds+4\Big[H_{11b}(x_1,t_1,p)+H_{11s}(x_1,t_1,p)\Big]\right\}, \tag{C4}$$

$$H_{11b}(x_1,t_1,p)=\int_0^\infty[k_{12}(\alpha,x_1,t_1,p)-k_{12\infty}(\alpha,x_1,t_1,p)]d\alpha, \tag{C5}$$

$$H_{11s}(x_1,t_1,p)=\frac{b_{11}}{(t_1+x_1)^2}+\frac{b_{12}}{t_1+x_1}+\frac{2b_{21}}{(2h_1+t_1+x_1)^3}$$
$$+\frac{b_{22}}{(2h_1+t_1+x_1)^2}+\frac{b_{23}}{2h_1+t_1+x_1}, \tag{C6}$$

$$H_{12}(x_1,t_2,p)=\frac{1+\kappa}{2\mu_0}\left\{H_{12b}(x_1,t_2,p)+H_{12s}(x_1,t_2,p)\right\}, \tag{C7}$$

$$H_{12b}(x_1,t_2,p)=\int_0^\infty[k_{13}(\alpha,x_1,t_2,p)-k_{13\infty}(\alpha,x_1,t_2,p)]d\alpha, \tag{C8}$$

$$H_{12s}(x_1,t_2,p)=\frac{b_{31}}{(x_1-t_2)^2}-\frac{b_{32}}{x_1-t_2}, \tag{C9}$$

$$H_{21}(x_2,t_1,p)=\frac{1+\kappa}{2\mu_0}\left\{H_{21b}(x_2,t_1,p)+H_{21s}(x_2,t_1,p)\right\}, \tag{C10}$$

$$H_{21b}(x_2,t_1,p) = \int_0^\infty [k_{22}(\alpha,x_2,t_1,p) - k_{22\infty}(\alpha,x_2,t_1,p)]d\alpha, \tag{C11}$$

$$H_{21s}(x_2,t_1,p) = \frac{b_{41}}{(x_2-t_1)^2} + \frac{b_{42}}{x_2-t_1}, \tag{C12}$$

$$\begin{aligned} H_{22}(x_2,t_2,p) = \frac{1+\kappa}{8\mu_0}\Bigg\{ & \int_0^A (k_{21}+k_{21c})\cos[s(t_2-x_2)]ds \\ & + \int_A^\infty (k_{21}+k_{21c} - \frac{4\beta_2 \ln \alpha_2 \mu_0}{s(1+\kappa)})\cos[s(t_2-x_2)]ds \\ & + \int_0^\infty (k_{21}-k_{21c}+\frac{8i\mu_0}{1+\kappa})i\sin[s(t_2-x_2)]ds + 4\Big[H_{22b}(x_2,t_2)+H_{22s}(x_2,t_2)\Big]\Bigg\}, \end{aligned} \tag{C13}$$

$$H_{22b}(x_2,t_2,p) = \int_0^\infty [k_{23}(\alpha,x_2,t_2,p) - k_{23\infty}(\alpha,x_2,t_2,p)]d\alpha, \tag{C14}$$

$$\begin{aligned} H_{22s}(x_2,t_2,p) = \frac{b_{51}}{(t_2+x_2)^2} + \frac{b_{52}}{t_2+x_2} + \frac{2b_{61}}{(2h_2-t_2-x_2)^3} \\ + + \frac{b_{62}}{(2h_2-t_2-x_2)^2} + \frac{b_{63}}{2h_2-t_2-x_2}. \end{aligned} \tag{C15}$$

Here, k_{11c} and k_{21c} are the complex conjugate of k_{11} and k_{21}, respectively.

References

Atkinson, C. (1975): Some results on crack propagation in media with spatially varying elastic properties. *International Journal of Fracture* 11, 619–628.

Aboudi, J.; Arnold, S.M.; Pindera, M.J. (1994): Response of functionally graded composites to thermal gradients. *Composites Engineering*. 4, 1–18.

Atluri, S.N.; Shen, S. (2002): The meshless local Petrov-Galerkin (MLPG) method: A simple & less costly alternative to the finite element and boundary element method. *CMES: Computer Modeling in Engineering & Sciences*, vol. 3, pp. 11–52.

Chen, Y.F.; Erdogan, F. (1996): The interface problem for a nonhomogeneous coating bonded to a homogeneous substrate. *Journal of The Mechanics and Physics of Solids* 44, 771–787.

Cook, T.S.; Erdogan, F. (1972): Stresses in bonded materials with a crack perpendicular to the interface. *International Journal of Engineering Science*. 10, 677–697.

Ching, H.K.; Batra, R.C. (2001): Determination of crack tip fields in linear elastostatics by the meshless local Petrov-Galerkin (MLPG) method. *CMES: Computer Modeling in Engineering & Sciences*, vol.2, no.2, pp. 273-289.

Ching, H. K.; Chen, J. K. (2006): Thermomechanical analysis of functionally graded composites under laser heating by the MLPG method. *CMES: Computer Modeling in Engineering & Sciences*, vol.13, no.3, pp. 199–217.

Choi, H.J. (2007a): Impact behavior of an inclined edge crack in a layered medium with a graded nonhomogeneous interfacial zone: antiplane deformation. *Acta Mechanica* 193, 67–84.

Choi, H.J. (2007b): Stress intensity factors for an oblique edge crack in a coating/substrate system with a graded interfacial zone under antiplane shear. *European Journal of Mechanics A-Solids* 26, 337–347.

Choi, H.J., Paulino, G.H. (2008): Thermoelastic contact mechanics for a flat punch sliding over a graded coating/substrate system with frictional heat generation. *Journal of The Mechanics and Physics of Solids* 56, 1673–1692.

Delale, F.; Erdogan, F. (1983): The crack problem for a nonhomogeneous plane. *Journal of Applied Mechanics* 50, 609–614.

Delale, F.; Erdogan, F. (1988): On the Mechanical modeling of the interfacial region in bonded half-planes. *Journal of Applied Mechanics* 55, 317–324.

Dag, S.; Erdogan, F. (2002): A surface crack in a graded medium under general loading conditions. *Journal of Applied Mechanics* 69, 580–588.

Ding, S.H.; Li, X. (2008a): Anti-plane problem of periodic interface cracks in a functionally graded coating-substrate structure. *Internaiton Journal of Fracture* 153, 53–62.

Ding, S.H.; Li, X. (2008b): An anti-plane shear crack in bonded functionally graded piezoelectric materials under electromechanical loading. *Computational Materials Science*, 43, 337–344.

Ding, S.H.; Li, X. (2008c): Periodic cracks in a functionally graded piezoelectric layer bonded to a piezoelectric half-plane. *Theoretical and Applied Fracture Mechanics* 49, 313–320.

Ding, S.H. (2009): Research on functionally graded material for fracture of collinear cracks and crack orientation angle and thermal stress problem. Ph.D. Thesis, Department of Mathematics, Shanghai Jiao Tong University.

Erdogan, F.; Gupta, G.D.; Cook, T.S. (1973): Numerical solution of singular integral equations. In:Sih, G.C, (Ed.), Mechanics of Fracture l: Mehtod of analysis and solution of crack problem. Noordhoff International Publishing, Leyden, The Netherlands, Chapter 7.

Erdogan, F.; Kaya, A.C.; Joseph, P.F. (1991): The mode III crack problem in bonded materials with a nonhomogeneous interfacial zone. *Journal of Applied Mechanics* 58, 419–427.

Erdogan, F.; Wu, B.H. (1996): Crack problem in functionally graded material layers under thermal stresses. *Journal of Thermal Stresses* 19, 237–265.

Erdogan, F.; Wu, B.H. (1997): The surface crack problem for a plate with functionally graded properties. *Journal of Applied Mechanics* 64, 449-456.

Guo, L.C.; Wu, L.Z.; Zeng, T.; Ma, L. (2004a): Mode I crack problem for a functionally graded orthotropic strip. *European Journal of Mechanics A-Solids* 23, 219–234.

Guo, L.C.; Wu, L.Z.; Ma, L.; Zeng, T. (2004b): Fracture analysis of a functionally graded coating-substrate structure with a crack perpendicular to the interface - Part II: Static problem. *International Journal of Fracture* 127, 39–59.

Guo, L.C.; Noda, N. (2008): Dynamic investigation of a functionally graded layered structure with a crack crossing the interface. International *Journal of Solids and Structures* 45, 336–357.

Hsueh, C.H.; Leeb, S. (2003): Modeling of elastic thermal stresses in two materials joined by a graded layer. *Composites Part B-Engineering* 34, 747–752.

Han,F.; Pan,E.; Roy,A.K.; Yue,Z. (2006): Responses of piezoelectric, transversaly isotropic, functionally graded and multilayered half spaces to uniform circular surface loading. *CMES: Computer Modeling in Engineering & Sciences*, vol. 14, pp. 15–30.

Jin, Z.-H.; Batra, R.C. (1996): Some basic fracture fracture mechanics condepts in functionally graded materials. *Journal of The Mechanics and Physics of Solids* 44, 1221–1235.

Kubair, D.V.; Bhanu-Chandar, B. (2007): Mode-3 spontaneous crack propagation along functionally graded bimaterial interfaces. *Journal of The Mechanics and Physics of Solids* 55, 1145–1165.

Li, C.Y.; Weng, G.J. (2001): Dynamic stress intensity factor of a cylindrical interface crack with a functionally graded interlayer. *Mechanics of Material* 33, 325–333.

Li, C.; Weng, G.J.; Duan, Z.; Zou, Z. (2001). Dynamic stress intensity factor of a functionally graded material under antiplane shear loading. *Acta Mechanica* 149, 1–10.

Li, Y.D.; Jia B.; Zhang, N.; Tang L.Q.; Dai, Y. (2006): Dynamic stress intensity factor of the weak/micro-discontinuous interface crack of a FGM coating. International *Journal of Solids and Structures* 43, 4795–4809.

Li, X. (2008): Integral equation. Science Press, Beijing.

Li, Y.D.; Kang Y.L.; Yao D. (2008a): Dynamic stress intensity factors of two collinear mode-III cracks perpendicular to and on the two sides of a bi-FGM weak-discontinuous interface. *European Journal of Mechanics A-Solids* 27, 808–823.

Li, Y.D.; Kang Y.L. (2008b). Fracture analysis of a weak-discontinuous interface in a symmetrical functionally gradient composite strip loaded by anti-plane impact. *Archive of Applied Mechanics* 78, 855–866.

Liu, D.; Yu, D. (2008): The coupling method of natural boundary element and mixed finite element for stationary Navier-Stokes equation in unbounded domains. *CMES: Computer Modeling in Engineering & Sciences*, vol. 37, no. 3, pp. 305–329.

Liu, D.; Zheng, X.; Liu, Y. (2009): A discontinuous galerkin finite element method for heat conduction problems with local high gradient and thermal contact resistance. *CMES: Computer Modeling in Engineering & Sciences*, vol. 39, no. 3, pp. 263–299.

Muskelishvili, I. N. (1953): Singular Integral Equations. Groningen: Noordhoff.

Ma, L.; Wu, L.Z.; Guo, L.C.; Zhou, Z.G. (2005): Dynamic behavior of a finite crack in the functionally graded materials. *Mechanics of Material* 37, 1153–1165.

Minutolo, V.; Ruocco, E.; Ciaramella, S. (2009): Isoparametric FEM vs. BEM for elastic functionally graded materials. *CMES: Computer Modeling in Engineering & Sciences*, vol. 41, no.1,pp. 27–48.

Oyekoya, O.; Mba, D.; El-Zafrany, A. (2008): Structural Integrity of Functionally Graded Composite Structure using Mindlin-type Element. *CMES: Computer Modeling in Engineering & Sciences*, vol.34, no.1, pp.55–85.

Sethuraman, R.; Rajesh, N. (2009): Evaluation of elastic-plastic crack tip parameters using partition of unity finite element method and pseudo elastic analysis. *CMES: Computer Modeling in Engineering & Sciences*,vol. 39, no. 1, pp. 67-99.

Sladek J.; Sladek V.; Zhang C. (2003): Application of Meshless Local Petrov-Galerkin (MLPG) Method to Elastodynamic Problems in Continuously Nonhomo-

geneous Solids. *CMES: Computer Modeling in Engineering & Sciences*, vol. 4(6), pp. 637-647.

Sladek, J.; Sladek, V.; Krivacek, J. (2005): Meshless local Petrov-Galerkin Method for stress and crack analysis in 3-d axisymmetric FGM bodies. *CMES: Computer Modeling in Engineering & Sciences*,vol. 8,no. 3,pp. 259–270.

Sladek, J.; Sladek, V.; Zhang, Ch.; Solek, P.; Starek, L.K. (2007): Fracture Analyses in Continuously Nonhomogeneous Piezoelectric Solids by the MLPG *CMES: Computer Modeling in Engineering & Sciences*,vol. 19, no. 3, pp.247–262.

Sladek, J.; Sladek, V.; Solek, P.; Wen, P. H.; Atluri, S. N. (2008): Thermal analysis of Reissner-Mindlin shallow shells with FGM properties by the MLPG. *CMES: Computer Modeling in Engineering & Sciences*, vol. 30, no. 2, pp.77-97.

Shin, S.; Huang, C.; Shiah, Y. (2009): Study of the underfill effect on the thermal fatigue life of WLCSP-Experiments and finite element simulations. *CMES: Computer Modeling in Engineering & Sciences*, vol. 40, no. 1, pp. 83-103.

So, W.M.G.; Lau, K.J.; Ng, S.W. (2004). Determination of Stress Intensity Factors for Interfacial Cracks Using the Virtual Crack Extension Approach. *CMES: Computer Modeling in Engineering & Sciences*,vol. 5,no. 3,pp. 189–200.

Wen, P.; Aliabadi, M.; Liu, Y. (2008): Meshless method for crack analysis in functionally graded materials with Enriched Radial Base Functions. *CMES: Computer Modeling in Engineering & Sciences*,vol.30,no. 3, pp.133-147.

Yu, D.; Huang, H. (2008): Theartificial boundary method for a nonlinearinterface problem on unbounded domain. *CMES: Computer Modeling in Engineering & Sciences*,vol. 35,no. 3,pp. 227-252.

Wang, B.L.; Mai, Y.W. (2006): A periodic array of cracks in functionally graded materials subjected to transient loading. *International Journal of Engineering Science* 44, 351–364.

Zuiker, J.; Dvorak, G. (1994): The effective properties of functinally graded composites-I. Extension of the Mori-Tanaka method to linearly varying fields. *Composites Engineering* 4, 19–35.

Zhou, Y.; Li, X.; Qin J. (2007): Transient thermal stress analysis of orthotropic functionally graded materials with a crack. *Journal of Thermal Stresses*, vol. 30, pp. 1211–1231.

Zhou, Y.; Li, X.; Yu, D. (2008): Integral Method for Contact Problem of Bonded Plane Material with Arbitrary Cracks. *CMES: Computer Modeling in Engineering & Sciences*, vol. 36,no. 2,pp. 147-172.

Zhou, Y.; Li, X.; Yu, D. (2009): Transient Thermal Response of a Partially Insulated Crack in an Orthotropic Functionally Graded Strip under Convective Heat Supply. *CMES: Computer Modeling in Engineering & Sciences*, vol.43, no.3, pp.191-221.